# FLUID-DYNAMIC EFFECTS ON THE RESPONSE OF OFFSHORE TOWERS TO WAVE AND EARTHQUAKE FORCES

by

ASOKE KUMAR SEN

B. Tech (Hons.), Indian Institute of Technology, Kharagpur, India, 1957

A THESIS SUBMITTED IN PARTIAL FULFILMENT OF

THE REQUIREMENTS FOR THE DEGREE OF

MASTER OF APPLIED SCIENCE

in the Department

of

CIVIL ENGINEERING

We accept this thesis as conforming to the required standard

THE UNIVERSITY OF BRITISH COLUMBIA

July, 1971

In presenting this thesis in partial fulfilment of the requirements for an advanced degree at the University of British Columbia, I agree that the Library shall make it freely available for reference and study. I further agree that permission for extensive copying of this thesis for scholarly purposes may be granted by the Head of my Department or by his representatives. It is understood that copying or publication of this thesis for financial gain shall not be allowed without my written permission.

Department of Civil Engineering

The University of British Columbia
Vancouver 8, Canada

Date July 19 , 1971

# ABSTRACT

The evaluation of fluid forces on vibrating framed structures in a fluid environment is of current significance in view of the activity in ocean engineering. Accurate knowledge of the fluid forces under conditions of variable separated flow is lacking. In this study an attempt has been made to find a general method of evaluation of fluid forces on cylinders for variable flow, using published data from tests of constant velocity flow, uniformly accelerated flow and wave motion. The parameters that appear to govern the variable flow forces are discussed, and models for relating force magnitudes to these parameters are suggested.

The dynamic response of framed structures in an ocean environment has not been investigated except for linear sinusoidal wave motion in deep water conditions. The response of shallow water structures to various types of wave forces, as well as to earthquake excitation, has been analysed numerically here, taking into account the interaction between the structure and fluid motions. The effect of the mass and drag parameters on the structure response has been studied. Governing load cases for the design of framed structures have been related to structural period and water depth.

# TABLE OF CONTENTS

# LIST OF TABLES

# LIST OF FIGURES

# ACKNOWLEDGMENT

The writer is indebted to his thesis supervisor, Dr. Donald L. Anderson for his inspiring and valuable assistance and guidance at every stage of this work. The work has been brought to this stage of compilation primarily because of his constant support and encouragement.

Financial support for the writer in the form of a research assistantship from an N.R.C. grant is also acknowledged.

# CHAPTER I

# INTRODUCTION

## 1.1 Scope:

The problem of vibrations induced in offshore structures by deep water waves has been extensively studied. In view of the increasing numbers of such structures being designed and constructed it was considered desirable to investigate the forces caused by other dynamic excitations, namely, an earthquake input and those ocean wave conditions which depart significantly from the assumptions of the linear small-amplitude wave theories. The magnitudes of the response to these kinds of excitation are compared with the response to linear deep water waves and with the response to breaking wave forces within the usual range of structures in shallow water. Tower-supported platform structures and similar framed structures only are considered. Attention has also been given to the problem of evaluation of the hydrodynamic forces under realistic water flow conditions.

## 1.2 Fluid interaction:

A flow diagram of the interaction between the water forces and the structural response is given in Fig. 1.

FLOW DIAGRAM

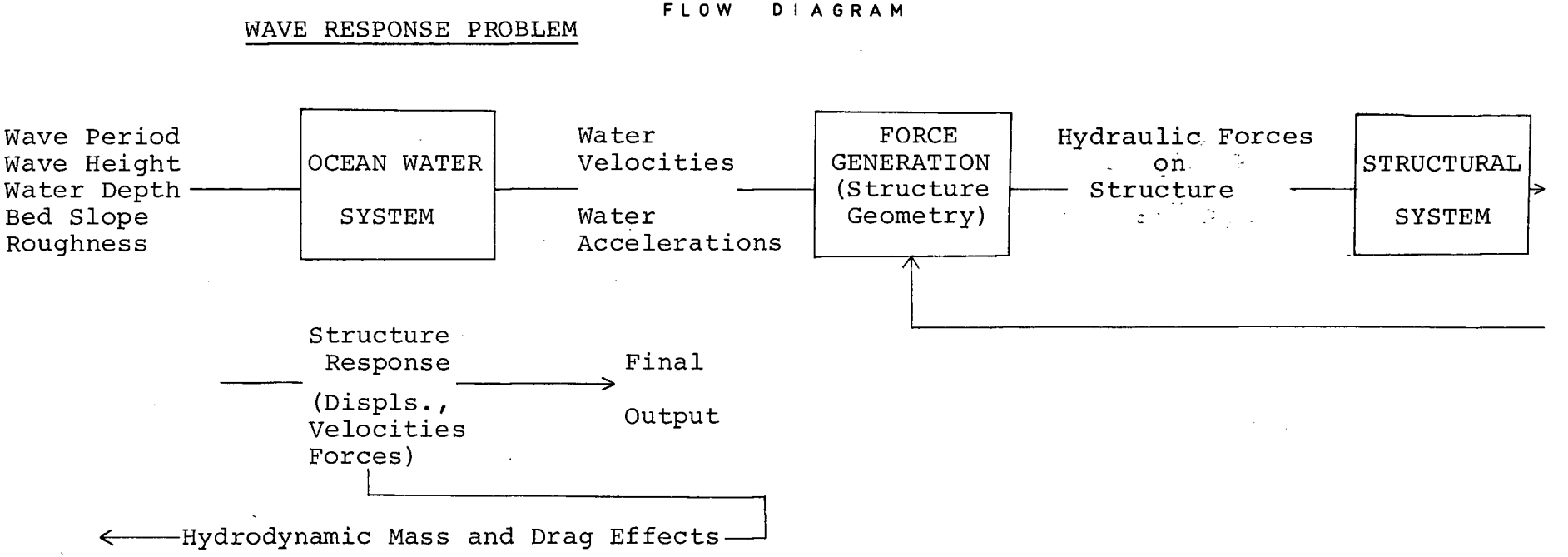


Fig. 1

## 1.3 Earthquake problem:

In the case of earthquake-caused vibrations, the force system consists primarily of the application, in effect, of recorded ground acceleration values to discrete masses. This equivalent dynamic force is fed into the linear structural system as an input. Since the structural motions cause an interaction with the water in the form of hydrodynamic drag and inertia forces, the final response is not the linear response, but is a function again of the hydrodynamic forces generated/influenced by the response. The hydrodynamic interactive forces attach themselves to the other inputted forces. Detailed expressions given later show that the hydrodynamic drag effects are nonlinear. In general the hydrodynamic inertia effects are also nonlinear.[11]

## 1.4 Wave problem:

The inputs required for the wave response problem differ in that the primary forces are caused by water motion relative to the structure motion. The water velocity and acceleration are calculated from one of several wave theories using inputs of wave period, wave height, water depth and the slope, roughness and configuration of the bed.

## 1.5 Simplifications:

Numerical studies have been conducted in both problems, taking the initial inputs as deterministic. The hydrodynamic

interaction forces were moreover simplified assuming two-dimensional transverse flow past circular cylinders to be applicable.

1.6 Organization of the thesis:

The second chapter is concerned with the determination of steady and unsteady fluid forces on cylindrical members when input data on the velocities and accelerations of the water particles relative to the member are supplied. The nature of the fluid-induced forces for steady flow is first discussed, followed by an examination of such forces for progressively increasing complexities of the flow in the unsteady area. Both theoretical (qualitative) and experimental evidence available relating to such forces are presented and the need for an experimental approach for the case of an arbitrary flow-history is highlighted. The dimensionless drag and mass coefficients for the forces are introduced and based on a reanalysis of past experimental data a relationship for the instantaneous mass coefficient is proposed in terms of the flow parameters.

The third chapter discusses the flow conditions created by various types of waves and includes a short description of the earthquake ground motion. This chapter presents quantitative information for the determination of fluid particle velocities and accelerations for different wave theories. The applicability of the various wave theories to varying conditions

of the ocean-structure geometry, etc. and the need for taking into account the various kinds of waves are set out.

The fourth chapter formulates the equations of motion of the structure under earthquake and dynamic wave force inputs.

The results of response computations under a) earthquake inputs, b) shallow water nonlinear oscillatory wave inputs, and c) breaking wave inputs are stated in detail in the fifth chapter. The response of the selected structures for varying values of drag, mass and other parameters are compared. The structure forces under various kinds of excitation and loading are compared.

In the last chapter, the conclusions and a summary of findings are given. The design criteria which would govern for various ocean-structure situations are indicated.

# CHAPTER II

## FLUID FORCES

This chapter is devoted to the determination of the forces on cylindrical members due to relative motion of the adjacent fluid. These forces are to be used in calculating the structure response. For cylindrical members the forces consist of a velocity-dependent drag component and an acceleration-dependent inertia force component. Dimensionless coefficients of drag and inertia appear within the constants of proportionality to the fluid velocities (to the second power) and the accelerations respectively. The kinematics of water motion being dealt with separately in the next chapter (Ch. III), the force problem reduces to the determination of drag and inertia characteristics for specific flow conditions.

Unsteady flow characteristics exist in both the earthquake and wave force situations. The motion has an arbitrary character in the former and is oscillatory, with occurrence of separation, in the latter. It is pointed out in the chapter that the drag and inertia in separated flow are time-dependent and not susceptible to an analytical solution. Methods used in the experimental determination of the average drag and average mass characteristics under specific types of unsteady flow as well as steady flow are indicated. The flow parameters used

in the determination of the coefficients of mass and drag are selected on the basis of dimensional analysis and regression of the existing experimental data.

## 2.1 Cylindrical pile force formula:

In computations for the forces on a cylinder due to waves and to other types of structure-fluid interaction, the total force is taken to be a superposition of drag and inertia forces such that[1]

$$F(t) = F_I(t) + F_D(t)$$

the forces being respectively

1) An inertia force $F_I(t)$ arising out of acceleration of the fluid and represented by an added mass.
2) A drag $F_D(t)$ comprising viscous friction and the portion of the pressure differential upstream and downstream due to the existence of the wake. In the range of Reynolds numbers of interest, this is proportional to the square of the velocity.

The above superposition concept is however true only for two-dimensional flow past cylinders.

Expressions for individual terms are:

$$F_I(t) = C_M \rho V_0 \frac{\partial v}{\partial t} \qquad (2.1)$$

$$F_D(t) = \frac{1}{2} C_D \rho A v|v| \qquad (2.2)$$

where $V_0$ = Enclosed volume of the member

$A$ = Projected area of the member

$v$ = Relative velocity between the member and the fluid particles assuming fluid particle velocity to be that of the undisturbed flow of the surrounding fluid.

$C_M$ = A dimensionless coefficient of mass

$C_D$ = A dimensionless coefficient of drag

$\rho$ = Mass density of the fluid.

## 2.2 Basic flow phenomena:

In order to gain greater insight into the drag and inertia forces, certain physical characteristics of fluid flow are examined in detail in this and succeeding sections. Discontinuous features of the flow appear in the case of motion of a real viscous fluid past a cylinder. First, in this section, steady flow is considered.

For real fluid flow, separation of the layer in contact with the boundary leads to the formation of vortices (Figs. 2 to 4). As velocity of flow is increased, it eventually results in their being detached, giving rise to a wake for a distance downstream of 1 to 4 diameters. The discharge of vortices [which when established constitute a Karman vortex street, Fig. 4] occurs, at a sufficiently high velocity, alternately from opposite edges of the cylinder at a frequency determined by the Strouhal number S given by

# SEPARATED FLOW PHENOMENA

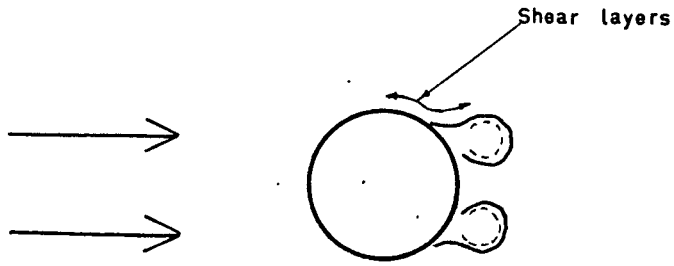


Fig 2

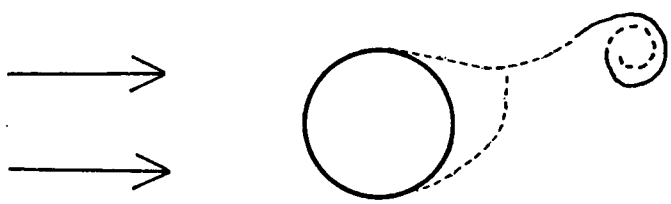

Fig 3

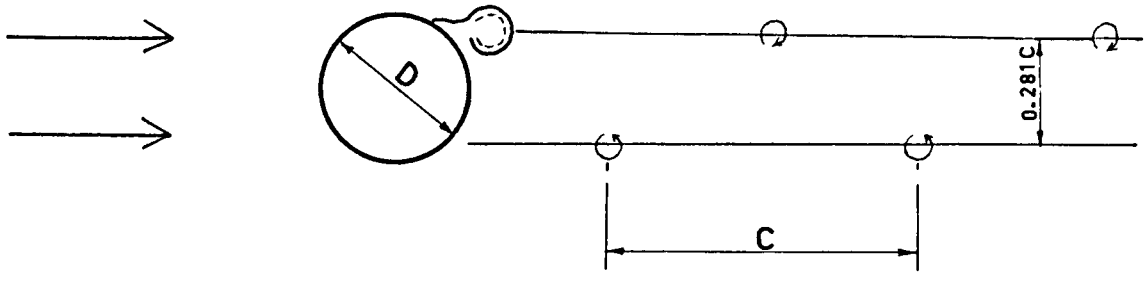


Fig 4

$$S \doteq S\left|1 - \frac{19.7}{N_R}\right| = \frac{fD}{v} \qquad (2.3)$$

where $f$ = frequency of shedding of a pair of eddies

$D$ = diameter

$N_R = \frac{vD}{\nu} = \frac{vD\rho}{\mu}$ = Reynolds number.

$\nu = \frac{\mu}{\rho}$ = kinematic viscosity.

Over the range of interest the number S is 0.21. The discontinuity represented in the wake downstream is bounded by shear layers starting from the separation points on the opposite edges of the cylinder and extending for the aforesaid distance downstream. The wake contributes to the pressure differential that brings about the major part of the drag; it also accounts for fluctuations in the drag from its mean value.

## 2.3 Drag fluctuations--steady flow:

In steady flow when the velocity is sufficiently high to lead to vortex-shedding, the mechanism for fluctuations in drag (and in lift) is indicated, with reference to the changing transient flow configuration in Fig. 5. Fluctuations in circulation and velocity are, according to Bernoulli's equation, accompanied by fluctuations in pressure, and hence in longitudinal drag. An individual vortex causes a complete cycle in the history of longitudinal forces (drag).[9,22,23] This occurs because the right and left vortices dissipate in a longitudinally identical wake (Fig. 5). The fluctuations in drag, which can

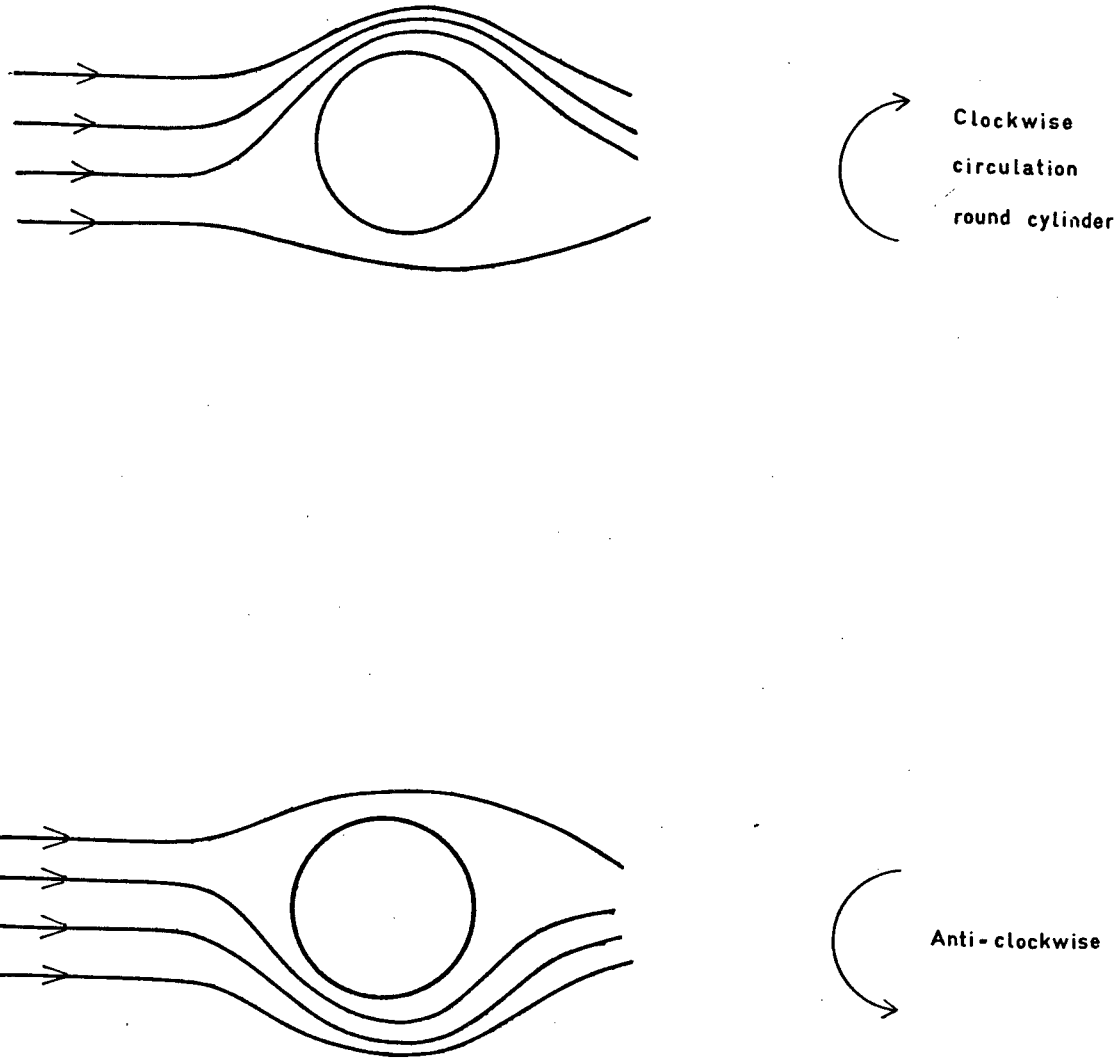


CIRCULATION AROUND CYLINDER

Fig 5

amount to as much as 60 percent of the mean drag, occur at a frequency of $\frac{1}{T_e}$ where $T_e$ = time for discharge of one eddy.[22]

2.4 Lift--steady flow:

A comment on lift forces in steady flow is in order. In the realm of post-separation velocities, arising out of the circulation around the cylinder (Fig. 5) lift forces are generated transverse to the flow, being proportional in magnitude to the square of the velocity and being of the order of the drag forces. The cyclic reversals of circulation described previously make the lift forces reverse cyclically at a frequency of $\frac{1}{2T_e}$ ("the Strouhal frequency"). Two stages of transverse asymmetry of the vortex layout are needed to complete a cycle in the lift force history.

2.5 Problems in unsteady flow:

Variability of the flow parameters is also found for flow with a time-dependent velocity. Observations are as follows:

a) The limiting $N_R$ for separation is time-dependent.

b) Positions along the boundary where separation occurs are time-dependent.

c) The wake geometry influences the drag more drastically. It is a function of velocity, cylinder diameter, viscosity and degree of turbulence.

d) Fluctuations of the instantaneous drag (and, in this type of flow, inertia forces) from its mean value are more irregular.

The complications involved in an attempt at analytical study can be seen from the fact that when the flow reverses, the erstwhile wake becomes the upstream side of the cylinder. Quantitative knowledge regarding the flow and forces is lacking for the general case of arbitrary acceleration (with separation).

2.6 $C_D$ - Coefficient of drag:

The following sections will be concerned with the characteristics of the coefficient $C_D$.

For steady flow a correlation between the drag coefficient $C_D$ and $N_R$ is well-established (Fig. 6). The characteristics of the experimental plot (Fig. 6) are as follows:

The drag coefficient is nearly constant at 1.2 in the practical range of

$$10^4 < N_R < 5 \times 10^5$$

except for a drop to a minimum of 0.4 for supercritical flows ($N_R > 2 \times 10^5$ approx.). It rises for low Reynolds numbers to a limit of 10.

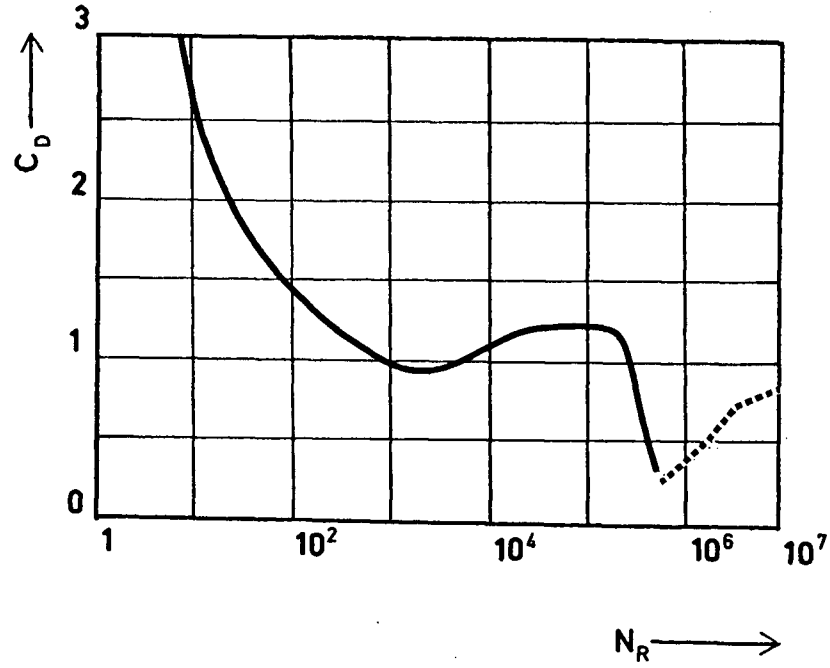


VARIATION OF $C_D$

Fig 6

## 2.7 Limits for the pre-separation stage and associated $C_D$ values:

While vortex-shedding in steady flow starts at an $N_R$ of the order of 50, the point of separation occurs at $N_R \doteq 1.2 \times 10^4$ in the case of constant acceleration starting from rest. Thus the instantaneous value of $N_R$ alone is not an adequate parameter for determining separation. The following two conditions are proposed as a means of predicting separation in variable flow:

i) oscillatory flow: parameter $\frac{v_{max}\ T}{D} = 15$, where D is the diameter and T the oscillation period.

ii) other: $N_R = 1000$ combined with an overriding limit of $\frac{s}{D} = 0.3$, where s = distance traversed on the current stroke.

The value of $C_D$ prior to separation is that due to friction drag alone and ranges from $C_D = 1$ to 2, as found by Keulegan,[10] for waves. In general, for waves and earthquakes the velocities in this range are low and so the force associated with drag is small compared to the inertia force; thus a high degree of accuracy is not required in this range.

## 2.8 Past experimental data:

An experimental approach has to be resorted to for forces in unsteady flow with separation. In succeeding sections

flow phenomena in specific types of unsteady flow as observed by past investigators are described--in order of increasing irregularity of motion and decreasing member rigidity. These observations yield an insight into the important flow parameters that influence forces. Such a knowledge of parameters is necessary so as to attempt to formulate a relation for inertia and drag forces in the case of a variable flow.

## 2.9 Experiments for $C_D$ in oscillatory waves:

Turning to the work of past experimenters on the wave motion type of unsteady flow, the drag coefficient $C_D$ has generally been evaluated by measuring the total force on a cylinder, immersed in the flow, at the instant the wave crest passes the cylinder. At this instant the water particle accelerations are theoretically zero and so the total force is equal to the drag force. The observed values of $C_D$ on this basis show wide scatter when plotted against $N_R$ (Fig. 7). The values of $C_D$ with the respective data sources are tabulated in Table 1. The disparities among these values are due to factors listed in Appendix I. It is also commented that roughness of the cylinders increases $C_D$ in the zone $N_R > 2 \times 10^5$.[3]

## 2.10 Rigid cylinders in standing waves--mean $C_D$:

McNown[13] has determined the influence of vortex-shedding on $C_D$ for <u>rigid model cylinders under standing waves</u>.

TABLE 1

WAVE FORCE COEFFICIENTS

[From Ref. 3]

| Experimenter and Date | | Diameter of Cylinder (in.) | $C_D$ | $C_M$ | Type of Flow |
|---|---|---|---|---|---|
| Crooke, 1955 | Model | $2, 1, \frac{1}{2}$ | 1.60 | 2.30 | Oscillatory |
| Keulegan & Carpenter, 1956 | " | $3, 2\frac{1}{2}, 2$ | 1.34 | 1.46 | " |
| | " | $1\frac{1}{2}, 1\frac{1}{4}$ | 1.52 | 1.51 | " (Standing Waves) |
| Keim, 1956 | " | $1, \frac{1}{2}$ | 1.00 | 0.93 | Accelerated, non-oscillatory |
| Dean, 1956 | " | 3 | 1.10 | 1.46 | " |
| Wiegel et al, 1956 | Prototype | 24 | 1.00 | 0.95 | Ocean waves California |
| Reid, 1956 | " | $8\frac{5}{8}$ | 0.53 | 1.47 | Ocean waves Gulf of Mexico |
| Bretschneider, 1957 | " | 16 | 0.40 | 1.10 | " |
| Wilson, 1957 | " | 30 | 1.00 | 1.45 | " |
| Paape, 1966 | Model | - | Variable with ratio $\frac{H}{D}$ | | |

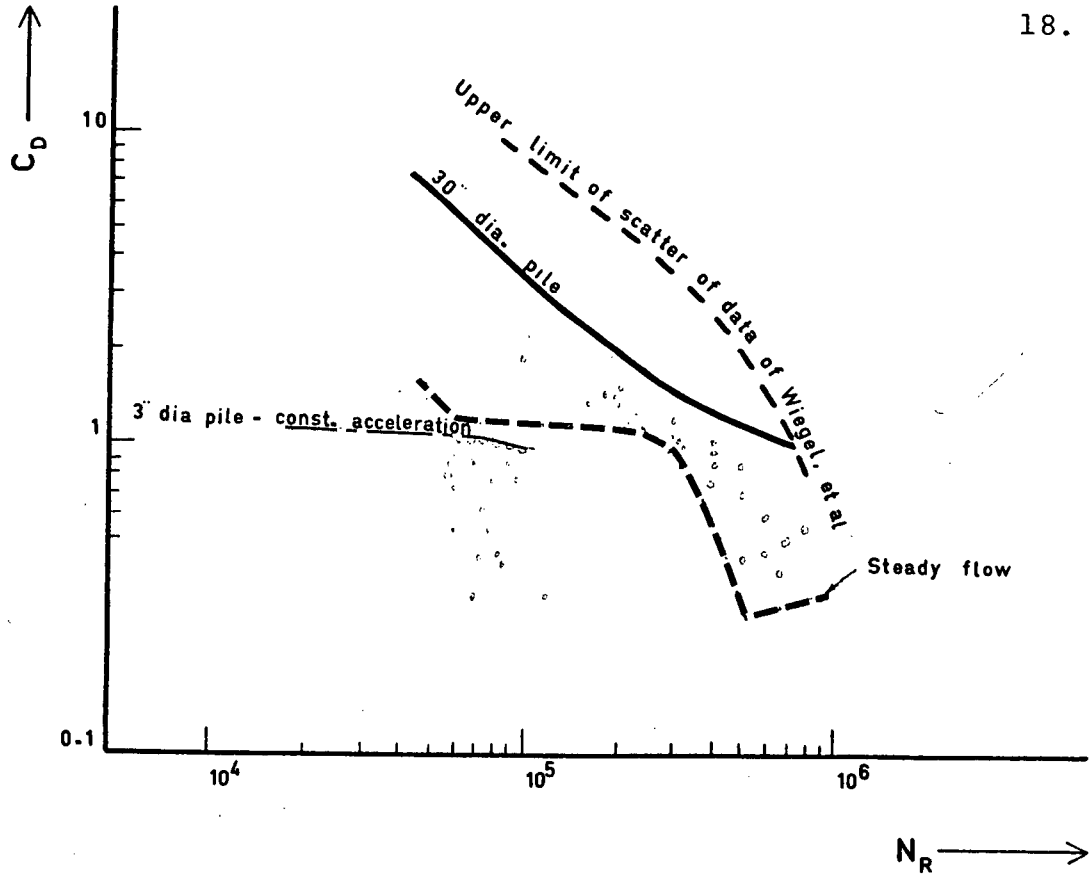


SCATTER OF VALUES OF $C_D$

Fig 7

The tests involved large amplitude water oscillations. Average values of $C_D$ have been given as a function of the parameter $\frac{T}{2T_e}$,

where $T$ = period of standing waves

$T_e$ = eddy-shedding period for the maximum velocity $v_{max}$.

Average $C_D$ falls steeply from 2.0 for $\frac{T}{T_e}$ in the neighbourhood of 2 to an ultimate value of 1.2 if $\frac{T}{T_e}$ is much different from 2. $\frac{T}{T_e}$ can be physically interpreted in terms of vortex-shedding and Strouhal number. This parameter $\frac{T}{T_e}$ alone however would not provide good correlation to $C_D$ for an arbitrary kind of unsteady flow.

2.11 Rigid cylinders in standing waves--varying $C_D$:

A specific analysis of the variation of drag and inertia forces at various instants in the cycle of oscillation was carried out by Keulegan and Carpenter.[10] The rigid model cylinder was placed at the node of standing waves, with flow conditions adjusted to ensure uniform horizontal velocity from the surface to the bottom. The tests involved large-amplitude water oscillations. Through a Fourier analysis of the measured forces, and assuming that the coefficients of higher harmonics were negligible, they evaluated $C_D$ at various instants throughout a cycle of oscillation (Table 2). The separation of the instantaneous values of $C_D$ and $C_M$ was effected as follows:

TABLE 2

VALUES OF $C_M$ AND $C_D$ FOR STANDING WAVES

(CYLINDERS)

| $\frac{V_M T}{D}$ | R.M.S. Average Over Cycle | | Instantaneous Values of $C_M$ & $C_D$ | | | | | | | | | | | |
|---|---|---|---|---|---|---|---|---|---|---|---|---|---|---|
| | | | $\frac{t}{T}$=0.2 | | $\frac{t}{T}$=0.4 | | $\frac{t}{T}$=0.5 | | $\frac{t}{T}$=0.6 | | $\frac{t}{T}$=0.8 | | $\frac{t}{T}$=1 | |
| | $C_M$ | $C_D$ | $C_M$ | $C_D$ | $C_M$ | $C_D$ | $C_M$ | $C_D$ | $C_M$ | $C_D$ | $C_M$ | $C_D$ | $C_M$ | $C_D$ |
| 3.0 | 2.14 | 0.70 | 2.05 | 1.6 | 2.1 | 0.9 | 1.9 | 0.4 | 2.1 | 0.9 | 2.05 | 1.6 | 2.0 | 0.4 |
| 15.6* | 0.80 | 2.05 | 1.2 | 2.1 | -0.3 | 1.9 | -2.0 | 2.0 | -0.3 | 1.9 | 1.2 | 2.1 | -1.4 | 1.9 |
| 44.7 | 1.76 | 1.54 | 1.9 | 1.5 | 2.1 | 1.4 | 2.2 | 1.6 | 2.1 | 1.4 | 1.9 | 1.5 | 2.2 | 1.4 |

*This corresponds to $\frac{T}{2T_e} = 1$

t = time from passage of crest.

Letting $T$ = the period of the flow oscillations

$F$ = total fluid force

and then using the fact of periodicity of F and the symmetry of the flow,

$$F\left(\frac{2\pi}{T}t\right) = -F\left(\frac{2\pi}{T}t + \pi\right) \tag{2.4}$$

The non-dimensionalised force $\frac{F}{\rho v_m^2 D}$ can accordingly be expressed as a Fourier series with respect to the variable t. The coefficients of the Fourier series are determined from measured values of the flow-induced forces. On the other hand the Morison expression for the fluid forces, namely,

$$\frac{F}{\rho v_m^2 D} = C_M \frac{V_o \frac{2\pi}{T}}{D v_m} \sin\frac{2\pi t}{T} + \frac{1}{2} C_D \left|\cos\frac{2\pi t}{T}\right| \cos\frac{2\pi t}{T} \tag{2.5}$$

(where $v_m$ = max. velocity)

can also be expanded as a trigonometric series. Like terms in the two trigonometric series are compared to yield series expressions for $C_D$ and $C_M$ as a function of t. Though $C_D$ is time-dependent, weighted average values over a wave cycle can be evaluated from an integral for the mean value. Furthermore expressing

$$F = f(t, T, v_m, D, \rho, \nu') \tag{2.6}$$

by means of dimensional analysis they obtained

$$\frac{F}{\rho v_m^2 D} = f\left(\frac{2\pi t}{T}, \frac{v_m T}{D}, \text{max. } N_R \equiv \frac{v_m D}{\nu}\right) \tag{2.7}$$

These experimenters went on to evaluate coefficient $C_D$ at various instants of the cycle from the computed coefficients of the series expressions already derived; this was done for a series of flow regimes represented by the parameter $\frac{v_{max}T}{D}$. Table 2 shows that over the range of time when the instantaneous velocities were non-zero, ($\frac{t}{T} \neq 0.25$), instantaneous values of $C_D$ did not vary significantly. Further by using the concepts of Strouhal number $\frac{fD}{v}$ and the parameter $\frac{v_mT}{D}$, it was established that when $\frac{v_mT}{D}$ was much smaller than 15, no eddies formed; that a single vortex was formed in each stroke when $\frac{v_mT}{D}$ reached 15 and that numerous eddies per stroke formed for large values of $\frac{v_mT}{D}$. Distinct variations in (mean values as well as cyclic fluctuations) $C_D$ occurred in these ranges. This is exemplified by the values in Table 2. Mean $C_D$ rose sharply from small $\frac{v_mT}{D}$ to a maximum of 2.2 at $\frac{v_mT}{D}$ = 15 and fell gradually for larger $\frac{v_mT}{D}$. There was excellent correlation found between mean $C_D$ and the parameter $\frac{v_mT}{D}$.

2.12 Limitations of varying $C_D$ values:

Factors that invalidate the applying of these values obtained in Section 2.11 to an oscillation problem are:

1) Deviation of the pattern of water oscillation from that of a standing wave.
2) Geometric similarity (ratio $\frac{\text{wave height}}{\text{diameter}}$) is unlikely to be the same in the prototype.

## 2.13 Tests on rigid model cylinders in constant acceleration flow:

For a non-reversing unsteady flow situation, $N_R$ again is not an adequate parameter, since separation is not dependent on velocity alone. This is due to the fact that it takes time from the start of motion for separation to occur and vortices to be formed. For uniformly accelerated motion from rest, plots of $C_D$ against the parameter $\frac{s}{D}$ were given by Sarpkaya and Garrison[11] (reproduced at Fig. 8), where s = current distance traversed from rest. The parameter $\frac{s}{D}$ was selected on dimensional considerations. The plot (Fig. 8) shows that $C_D$ is low at small $\frac{s}{D}$ and reaches a maximum at $\frac{s}{D} \doteq 2.5$ at which there was a symmetric vortex configuration. It decreases to 1.0 at the shedding of the first vortex (asymmetric vortex pattern) around $\frac{s}{D} = 4.8$; it thereafter eventually attains a value of 1.2 at large $\frac{s}{D} \doteq 6$ to 7, the variations in $C_D$ occurring only during the first two vortices. This highlights the time taken for traversing an adequate distance in a stroke for the wake to form and for $C_D$ to assume separated flow values. No correlation of $C_D$ with $N_R$ or $\frac{v_m T}{D}$ was found.

## 2.14 $C_M$ - Coefficient of mass:

In this and succeeding sections the past data on experimental values of $C_M$ for particular cases of unsteady flow will be summarised. The theoretical value for inviscid irrotational flow is 2.0. For wave inputs on model and prototype

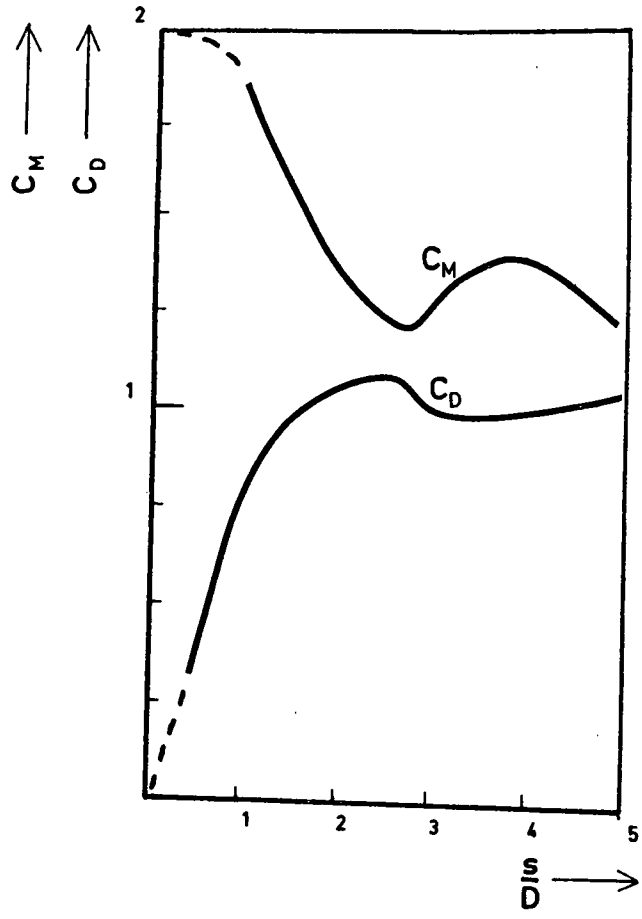


Fig 8

VARIATION OF $C_M$ AND $C_D$ WITH $\frac{S}{D}$

piles (rigid piles), Table 1 indicates values of $C_M$ from 0.95 to 2.3 (Appendix I details the reasons for the scatter). The coefficient was evaluated therein using the following approach:

> At the instant the level of the wave surface is at the still water level, the velocities are theoretically zero and the force is purely an inertia force. The measured force at this instant yields a value of $C_M$. This value is then assumed to be constant for subsequent predictions/computations of wave force.

In view of the scatter of the data available so far, judgment must be exercised in selecting $C_M$, taking into consideration the similarity of conditions in a given situation to those which prevailed in an experiment.

2.15 Rigid cylinders in standing waves--mean $C_M$:

Experiments on rigid model cylinders under standing waves to examine the influence of the vortex-shedding frequency on $C_M$: Paralleling section 2.10, the results of McNown from these experiments show that average $C_M$ falls from a value of 2 at low $\frac{T}{T_e}$ to a minimum of 1 at $\frac{T}{T_e} \doteq 2$ to 3. It increases again with large $\frac{T}{T_e}$ to 2, i.e., there is a definite correlation with parameter $\frac{T}{T_e}$.

2.16 Rigid cylinders in standing waves--varying $C_M$:

Experiments for instantaneous $C_M$ for rigid model cylinders in standing waves (Keulegan and Carpenter[10]): Section 2.11 has indicated that instantaneous values of $C_M$ were segregated in a series form, with respect to the time variable $\theta = \frac{2\pi t}{T}$. The expression for the instantaneous $C_M$ was found to be directly proportional to $\frac{v_m T}{D}$. The computed values of the time-dependent $C_M$ at various cycle points are given in Table 2; they show that $C_M$ values fluctuate more markedly than $C_D$ values, specially when $\frac{v_m T}{D} = 15$. Also, weighted average values of $C_M$ over a wave cycle were found from the expression

$$\bar{C}_M \equiv \frac{1}{\pi} \int_0^{2\pi} C_M(\theta) \sin^2\theta d\theta = \frac{2}{\pi 3} \frac{v_m T}{D} \int_0^{2\pi} \frac{F \sin\theta d\theta}{\rho v_m^2 D} \qquad (2.8)$$

where, in framing the expression for $C_M$ as a $\theta$-series, the higher order terms have been neglected. The parameter $\frac{v_m T}{D}$ is seen to influence $C_M$ directly, a conclusion which is also arrived at by dimensional analysis (Section 2.11). Mean values of $C_M$ during a cycle were correlated strongly with $\frac{v_m T}{D}$ and distinct variations in $C_M$ occurred for specific bands of values of $\frac{v_m T}{D}$. Mean $C_M$ sharply falls from 2.1 at low $\frac{v_m T}{D}$ to a minimum of 0.8 at $\frac{v_m T}{D} = 15$. It then rises gradually for larger $\frac{v_m T}{D}$. The parameter $\frac{v_m T}{D}$ was indicated to be important in any regression. The values obtained should be interpreted with caution as some computed values of $C_M$ are negative (physically impossible) as Table 2 shows.

2.17 Experiments on rigid model cylinders under constant acceleration from rest:

Section 2.13 indicated that for $C_D$ there was no correlation with $N_R$ or $\frac{v_m T}{D}$ in this flow. As expected this also holds true for $C_M$. Plots of $C_M$ against the parameter $\frac{s}{D}$ (due to Sarpkaya and Garrison: Fig. 8) show strong correlation. This highlights the time taken in traversing an adequate distance in a stroke for $C_M$ values to drop from 2.0 at rest to a lower ultimate value. At the start of motion when the relative flow is virtually irrotational, $C_M$ assumes the value 2, which decreases thereafter with increasing $\frac{s}{D}$ to 1.2. The $C_M$ curve rises again, reaching an asymptotic value of 1.3.

2.18 Oscillated flexible cylinders--mean resistance:

The results of a test for the measurement of combined drag and inertia forces are mentioned next.

The tests were conducted in the laboratory with single <u>flexible</u> model cylinders oscillated at large amplitudes in still water. Laird[9,21,22] investigated the forces for large amplitudes of longitudinal oscillations ($\frac{a}{D} >> 1$) within the region $2 \times 10^3 < N_R < 4 \times 10^4$ which fell within the practical range of flow. He found large increases in the <u>fluctuating intensity</u> of the total force over those on rigid cylinders of the order of up to 5 times (Fig. 9). Combined resistance (drag + inertia) was measured and reported, but the drag predominated. The <u>average</u>

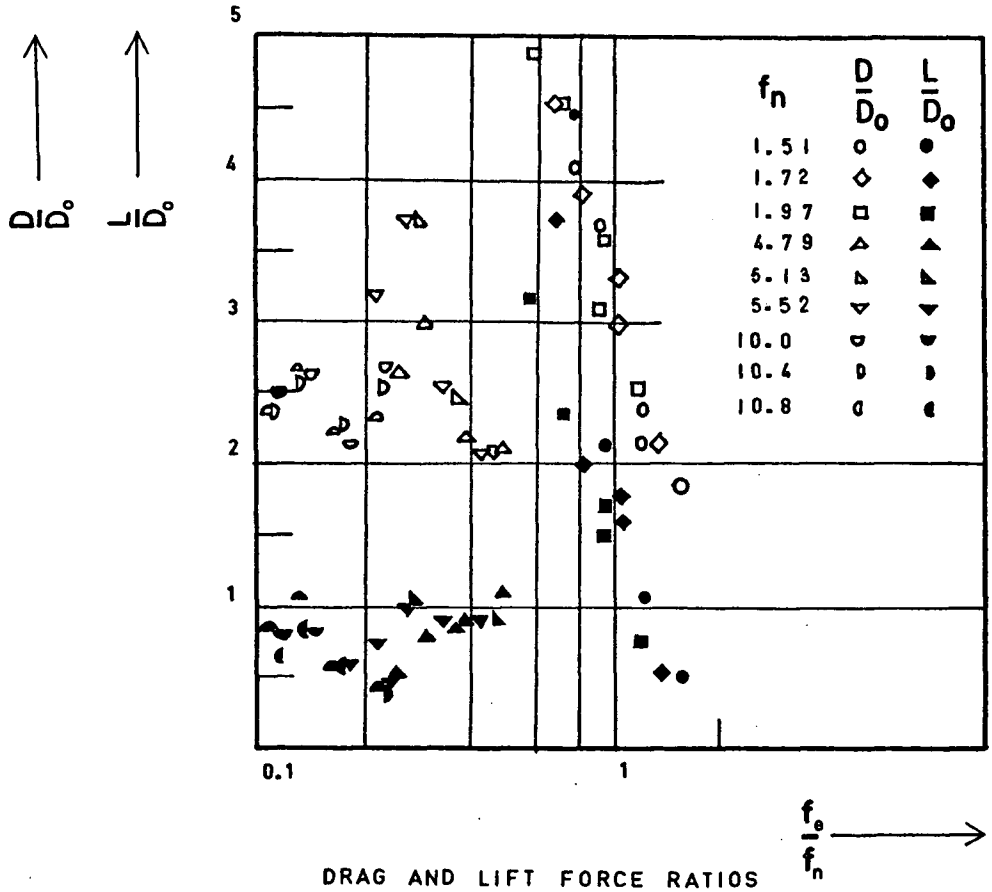


DRAG AND LIFT FORCE RATIOS

Fig 9

resistance forces were found to increase by about 3 to 4 times the steady-state drag $D_o$. Laird interpreted the unsteady flow forces in terms of the flow phenomena at various values of the parameters $\frac{f_e}{f_n}$ and $\underline{f}$

where $\underline{f}$ = forced oscillation frequency of the cylinder (This influences mean oscillation speed and hence the Strouhal frequency $f_e$).

$f_n$ = natural frequency of the flexible model in air.

$f_e$ = Strouhal frequency.

Fig. 9 highlights the amplification in fluctuating total drag for values of $\frac{f_e}{f_n}$ near unity. Based on the data for the 3 oscillators with $f_n$ = 1.51, 1.72 and 1.97 respectively, Laird has stated that as $f_e$ is reduced from a value equal to $f_n$, so long as the reduction is small, the maximum variable drag does not decrease. An explanation offered is that in these slower runs (smaller $f_e$ corresponding to smaller $\underline{f}$), there is greater time for the structural amplitude to increase during each stroke.

The force increases over those for rigid cylinders were attributed to lateral oscillations induced by fluctuating lift forces and to the increase in the wake widths which the lateral oscillations caused. When the maximum fluctuating lift was relatively high, the total resisting force was correlated directly to the square of the wake widths. Drag predominated

over inertia in these tests, though no separate values of the drag and inertia forces are available.

Structures should be designed to have a flexibility lower than what would significantly raise the fluid forces (i.e., magnify $C_D \gg 1.2$); from Fig. 9 the $\frac{f_e}{f_n}$ ratio should be less than 0.3. Practical structures with braced cylindrical piles fall within this category.

2.19 Lift in flexible oscillating cylinders:

The preceding experiments of Laird[9,21,22] concerning oscillations with large amplitudes show lift forces to be significant when the Strouhal frequency is close to or lower than $f_n$ ($\doteq 0.6\ f_n$ to $f_n$). A possible cause for the above effect when $f_e$ was less than $f_n$ would be the transfer of energy from the secondary drag oscillations at a frequency of $2f_e$. From the relationship $f_e = 0.21\ \frac{V}{D}$, it is seen that for the practical wave flow velocities of less than 12 ft./sec. (r.m.s.), the above lift effects would not be significant for the usual diameters of 1 to 3 ft. and structural frequencies of 0.3 to 1 cycles/sec. The extreme cases warranting examination of lift would be piles of small diameters under waves of large heights. Furthermore lift effects are ruled out in the earthquake case since the distance travelled in each stroke is not sufficient to cause prolonged eddy shedding.

The magnitudes of lift in the shallow water case with small-diameter piles are about those of drag.

2.20 Framing of relations for the instantaneous variable drag and mass coefficients (separated flow):

For cases of arbitrary accelerative motion, it is necessary to recognise the most important parameters that influence the value of $C_D$ and $C_M$, and to have recourse to experimental data to determine the correlation. An insight into the important variables has been offered by the experimental work described in Sections 2.9 to 2.18.

2.21 Choice of parameters:

The technique of dynamical similarity has been used to select dimensionless parameters that would correlate experimental values of the drag and inertia coefficients. Derivations given by Morison[4] and Crooke may be referred to.

2.22 Empirical coefficient of mass in arbitrary motion related to dimensionless parameters:

Some variables influencing $C_M$ after the onset of separation are:

1) Acceleration of the body
2) Acceleration in the surrounding fluid due to the presence of the body--depends on boundary configuration

3) Duration of the acceleration

4) Rate of change of the acceleration

5) Interaction of the velocity and

   i) the distance traversed on the current stroke

   ii) the time elapsed on the current stroke

6) Residual vorticity from previous cycles of oscillation

7) Symmetric or non-symmetric nature of vortex formation--related to Strouhal number.

Item number 4) could not be explicitly taken into account in the parameters chosen. Examining the relevant parameters, the most important of the basic variables influencing the value of $C_M$ are:

L = length parameter

v = velocity of the body

A = local acceleration

T = time parameter

Dimensional analysis was carried out, leading to two parameters being found to influence $C_M$:

$$C_M = C_M \left(\frac{AT^2}{L}, \frac{vT}{L}\right) \qquad (2.9)$$

Physical significance of parameters:

$\frac{AT^2}{D}$: a measure of

$$\frac{(\text{Local inertia}) \times (\text{Viscous force})^2}{(\text{Convective inertia})^3}$$

$\frac{vT}{D}$, taken in conjunction with $\frac{AT}{v}$, represents the ratio $\frac{\text{Convective inertia}}{\text{Local inertia}}$. The broad effect of variations in $\frac{vT}{D}$ on $C_M$ is that an increase in $\frac{vT}{D}$ increases $C_M$ when T is large and v is low.

A reanalysis of the experimental data in Section 2.16 and 2.17 disclosed that the instantaneous value of $C_M$ was adequately determined as a quadratic surface in the $\xi$-$\eta$-$C_M$ space, where

$$\xi = 0.125 \text{ Log}_{10}\left|\frac{10AT^2}{D}\right| + 0.985\left|\frac{vT}{D}\right| - 4.11$$

$$\eta = -\text{Log}_{10}\left|\frac{10AT^2}{D}\right| + 0.124\left|\frac{vT}{D}\right| + 0.903 \qquad (2.10)$$

T being the time elapsed from the start of the current stroke. The best regressive relation found was:

$$C_M = 1.35 + 0.026\,\xi^2 - 0.152\xi + 0.62\eta^2 \qquad (2.11)$$

Fig. 10 shows the variation of $C_M$ with the two parameters Log $\frac{10AT^2}{D}$ and $\frac{vT}{D}$ in the range covered by the tests. The values of $C_M$ as predicted by the equation and as experimentally observed are shown for specific data. The test results for constant acceleration all showed good correlation, while only

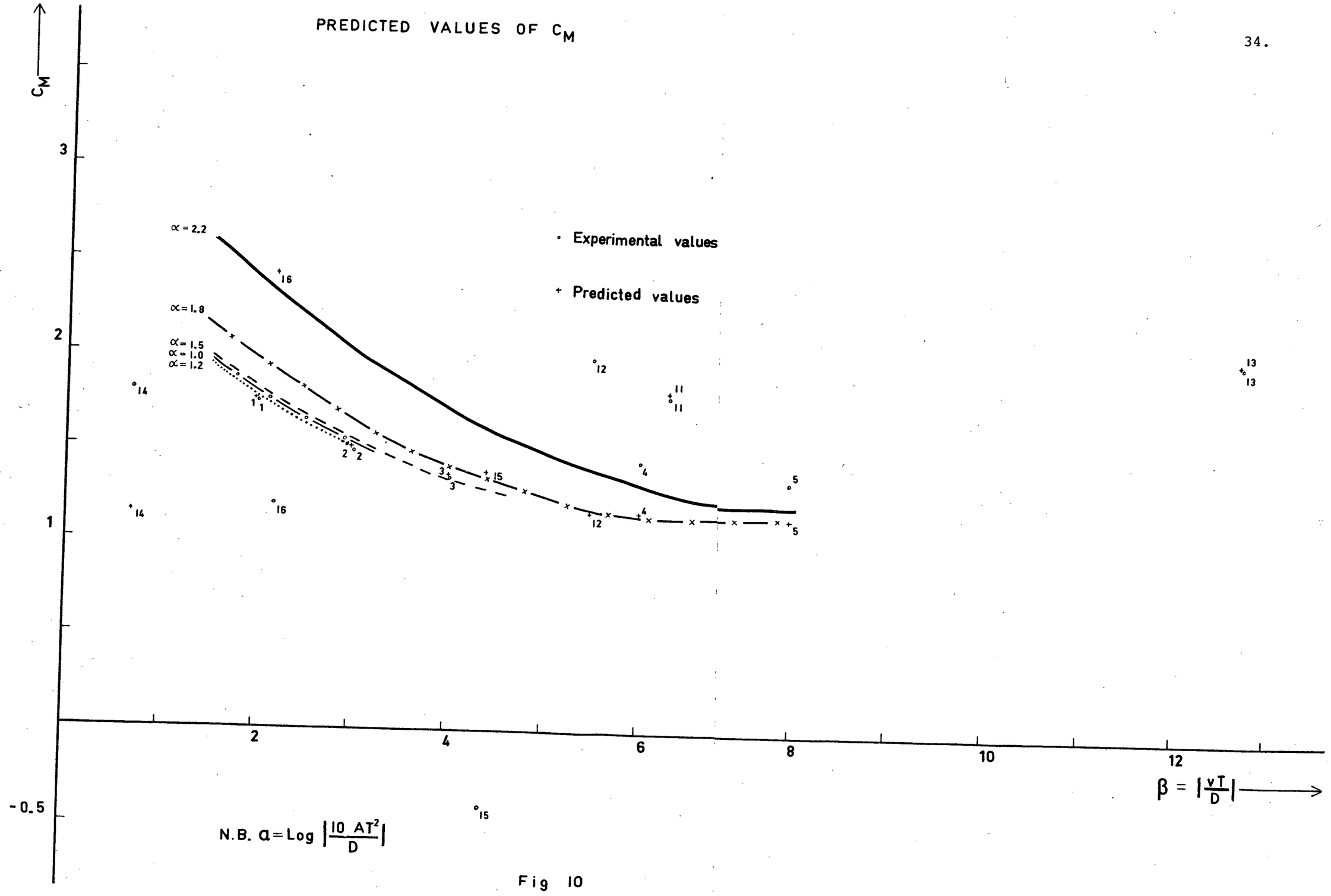
PREDICTED VALUES OF $C_M$
$C_M$
3
2
1
-0.5
$\alpha = 2.2$
$\alpha = 1.8$
$\alpha = 1.5$
$\alpha = 1.0$
$\alpha = 1.2$
• Experimental values
+ Predicted values
2
4
6
8
10
12
$\beta = \left|\frac{vT}{D}\right|$
N.B. $\alpha = \text{Log}\left|\frac{10\ AT^2}{D}\right|$

Fig 10

a few of the oscillatory flow test results diverged to an appreciable extent.

The choice of $\xi$ and $\eta$ as independent variables instead of $|\frac{10AT^2}{D_2}|$ and $|\frac{vT}{D}|$ enabled elimination of cross-product terms in $\frac{10AT^2}{D}$ and $\frac{vT}{D}$. The $\xi$-$\eta$ space representation involved a rotation of the orthogonal axes $|\frac{10AT^2}{D}|$ and $|\frac{vT}{D}|$, the rotation being small, i.e., $\sin^{-1}(0.125)$. $C_M$ given by equation (2.11) is valid in the range bounded by the following inequalities:

$$1.088 < (0.99 \text{ Log}_{10} |\frac{10AT^2}{D}| - 0.15 |\frac{vT}{D}|) < 2.1 \quad (2.12)$$

$$0.8 < \text{Log}_{10} |\frac{10AT^2}{D}| < 3 \quad (2.13)$$

$$0.7 < |\frac{vT}{D}| < 14 \quad (2.14)$$

In practice flow parameters would usually be within the ranges of the expressions given by (2.12), (2.13) and (2.14).

2.23 Empirical coefficient of drag in arbitrary 2-D motion (with separation):

Although a dimensional analysis approach similar to that for $C_M$ was followed, it was not found possible to formulate an empirical expression for $C_D$ that satisfactorily correlated the experimental values. The significant variables influcncing the coefficient of drag after separation occurs are:

i) Degree to which the wake has been established

2) Symmetry of vortices

3) Instantaneous value of circulation--this is related to viscosity, velocity and density
4) Fluid shear at the boundary of the body
5) Nearness of the frequency of cylinder motion to Strouhal frequency
6) Residual vorticity from previous cycles--related to 3)

Treating these as being represented in the variables $L, v, A, T, \mu$ and $\rho$, $C_D$ is found by dimensional analysis to be a function of the following (factor no. 5 above could not be explicitly taken onto account)

$$N_R, \frac{AL}{v^2} \text{ and } \frac{vT}{L} .$$

where $N_R$ is a measure of $\frac{\text{Convective inertia}}{\text{Viscous forces}}$

$\frac{AL}{v^2}$ is a measure of $\frac{\text{Local inertia}}{\text{Convective inertia}}$

$\frac{vT}{L}$ (ref. section 2.22) is an indirect measure of $\frac{\text{Convective inertia}}{\text{Local inertia}}$.

In an alternative choice of dimensionless parameters, $C_D$ is a function of:

$$\frac{\mu v T^2}{\rho D^3} , \frac{vT}{D} \text{ and } \frac{AT^2}{D}$$

where $\frac{\mu v T^2}{\rho D^3}$ is a measure of $\frac{(\text{Viscous force}) \times (\text{Convective inertia})}{(\text{Local inertia})^2}$

$$\frac{AT^2}{D} \text{ is a measure of } \frac{(\text{Local inertia}) \times (\text{Viscous forces})^2}{(\text{Convective inertia})^3}$$

As stated previously, regression carried out on the past experimental data did not give close agreement for the many proposed relationships, the data being meagre. Further experimental data is needed before a valid expression for $C_D$ can be proposed.

2.24 Force reductions due to neighbouring cylinders:

Reduction of wave forces on a trailing cylinder owing to the presence of a leading neighbour amounted to only 15 percent for a clear spacing of 3 diameters and 45 percent for a clear spacing of 1 diameter (vide tests by Laird,[20,21,23]). No reductions or alterations in drag forces are therefore justified in practical tower structures where the spacing is in most cases greater than 4 diameters.

# CHAPTER III

# WAVE THEORIES

In the previous chapter methods have been presented for the determination of the fluid forces on a member if the relative velocity and acceleration between the fluid particles and the member are known. In order to meet the latter requirement, this chapter is concerned with laying out the necessary information for determining the fluid motion in waves, or the ground motion in an earthquake situation.

## 3.1 Wave theories:

For tower structures in the oceans as well as wharves one of the major design criteria is the lateral force resulting from wind-generated waves, and occasionally single waves such as Tsunamis. Many investigators have worked on the problem of predicting the magnitude and frequency of wave motions[1,2] and the resulting fluid particle velocities.[1,2,3] Because of the many variables influencing wave geometry and water kinematics, a general theory for the mechanics of water waves in an arbitrary situation would be very complicated. In order to obtain, with a reasonable amount of effort, fairly accurate estimates of fluid particle velocity and acceleration under some of the more common regimes of flow, various simplified wave theories have been formulated. Some of the factors that determine the wave theory appropriate for use are:

- depth of water
- fetch, i.e., exposed length of water
- wind conditions
- slope of beach.

For any one location which determines depth, fetch and beach slope, different wind velocities produce waves of different heights and frequencies. The structural designer must then determine which condition is most severe for the proposed structure, taking into account the differing force and response levels for different structural frequencies.

In the following proposed wave theories expressions for particle motion will be presented which require prior knowledge of at least two parameters. The most common ones used are the wave height H (measured from trough to crest) and the period T, the time between the passage of successive waves. Thus we must be able to determine H and T from knowledge of the local conditions of wind speed, fetch, depth, beach slope and wind duration.

3.2 Wave height and period:

Methods for the evaluation of the wave height H and the period T in the deep water situation will now be considered. Relationships for wave height and period for waves generated in shallow water are available in ref. 6. In deep water, where $\frac{d}{L} > \frac{1}{2}$ (d being the water depth and L the wave length), the

principal parameters that influence the wave height H and the wave period T of wind-generated waves are the mean wind speed U, the fetch length F and the wind duration t. By dimensional analysis it can be shown that, neglecting less important parameters, the following relations must hold

$$\frac{gT}{U} = f_1\left(\frac{gF}{U^2}, \frac{gt}{U}\right)$$

$$\frac{gH}{U^2} = f_2\left(\frac{gF}{U^2}, \frac{gt}{U}\right).$$

The nature of the functions $f_1$ and $f_2$ have been determined empirically for the limiting cases of infinite t (depicted in Fig. 11) and of infinite F [expressed in eqns. 3.4]. For example, for infinite duration t, Fig. 11 shows an increase in height and period with wind velocity and fetch as would be physically expected.

For large time duration t, steady-state conditions are in effect reached and the wave height H and period T depend upon the Froude number $\frac{gF}{U^2}$. This is the fetch-limited case. Regression on experimental data gives the curves of $\frac{gH_{1/3}}{U^2}$ and $\frac{gT_{1/3}}{U}$ versus $\frac{gF}{U^2}$ shown in Fig. 11.

Here $H_{1/3}$ = significant wave height, i.e., average of the upper 1/3 values of H.

$T_{1/3}$ = significant period, similarly defined.

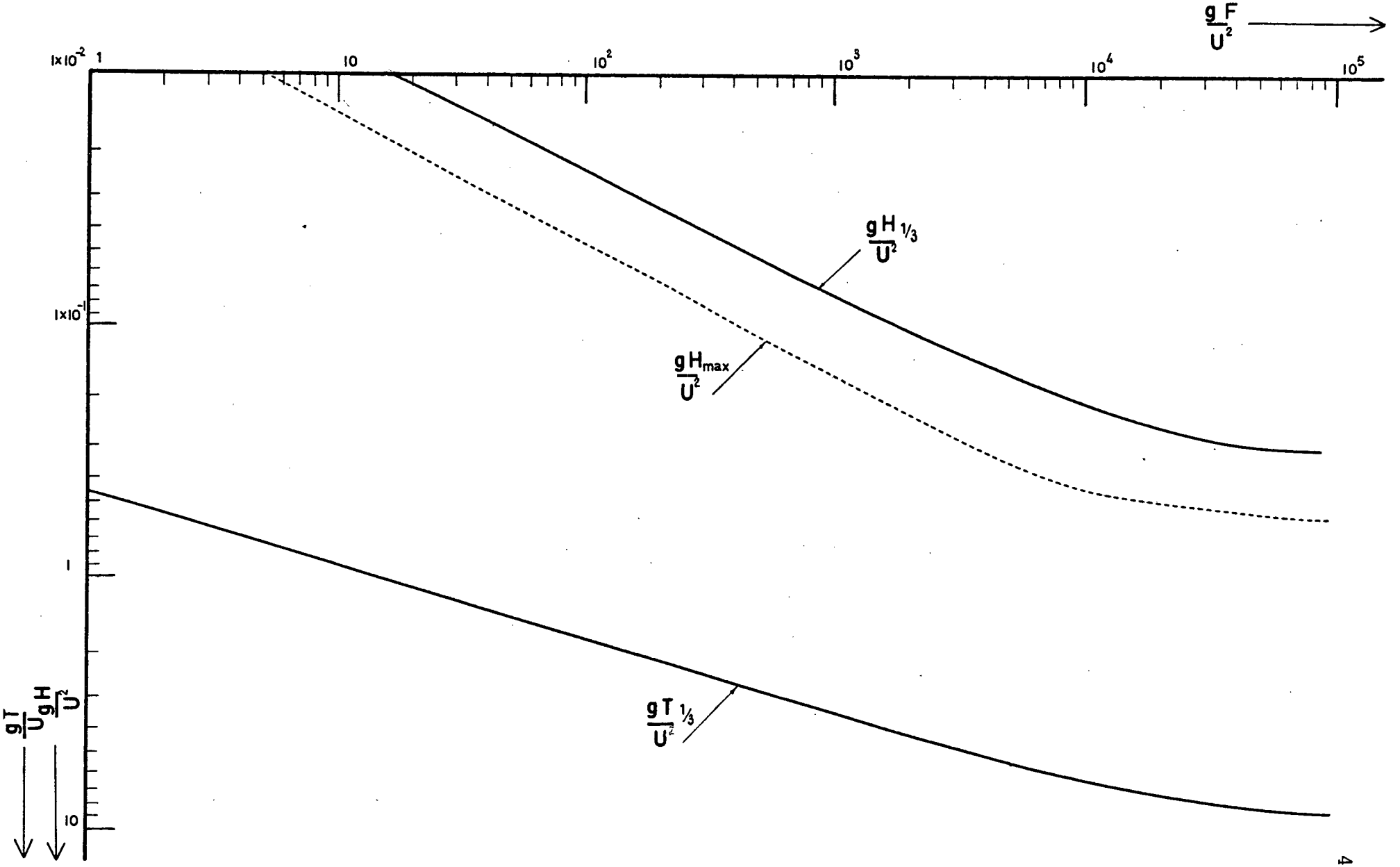


WAVE HEIGHT AND PERIOD

Fig II

In the zone $\frac{gF}{U^2} < 10^4$ the relations for H and T are nearly linear on log-log plots and so reduce to

$$H_{1/3} = 0.045\ UF^{0.5} \tag{3.1}$$

$$T_{1/3} = 0.6\ U^{0.4}F^{0.3} \tag{3.2}$$

where the units are

U = surface wind speed in m.p.h.

F = fetch length in miles

$H_{1/3}$ = height in feet

$T_{1/3}$ = period in seconds

For $\frac{gF}{U^2} > 10^5$, $\frac{gH_{1/3}}{U^2}$ becomes asymptotic to about 0.35 and $\frac{gT_{1/3}}{U}$ becomes asymptotic to 9. This corresponds to the case of a very large fetch and shows that in the practical range, an increase of fetch beyond 100 miles has no influence on the waves. From the approximate empirical relation[6] (p.3)

$$H_{max.} = 1.87\ H_{1/3}$$

the maximum design wave height becomes

$$H_{max.} = 0.084\ UF^{0.5}$$

$$\left[\text{valid for } \frac{gF}{U^2} < 10^4\right] \tag{3.3}$$

For the other case of a duration-limited wind wave, regression points to the following:

$$H_{1/3} \propto U^{1.5} \text{ to } U^{1.6}$$

and $$H_{1/3} \propto t^{0.4} \text{ to } t^{0.5} \qquad (3.4)$$

$$T_{1/3} \propto U^{0.7}$$

and $$T_{1/3} \propto t^{0.3}$$

(Ref. 1)

Approximate expressions valid in the range $20000 < \frac{gT}{U} < 500000$ are as follows:

$$H_{1/3} = 0.005\ t^{0.4}\ U^{1.6}$$

$$T_{1/3} = 0.006\ t^{0.3}\ U^{0.7} \qquad (3.5)$$

Here t = duration in seconds

U = surface wind speed in ft./sec.

Again for large t, $\frac{gH_{1/3}}{U^2}$ and $\frac{gT_{1/3}}{U}$ tend to constant values independent of $\frac{g.t}{U}$. $H_{1/3}$ and $T_{1/3}$ increase faster with the wind velocity U in this case compared with the fetch-limited case.

3.3 Ranges of applicability:

The various wave theories to be made use of in the appropriate ranges of flow conditions are as follows:

a) Linear small-amplitude theory, which is limited to the situation $\frac{d}{L} > \frac{1}{2}$ (i.e., $\frac{d}{T^2} > 2.5$ ft./sec.$^2$)

(vide Appendix II). A plot of L versus T for this theory is given in Fig. 12. The ratio of L to the length $L_0$ for infinite depth ($L_0 = gT^2/2\pi$) is plotted against $\frac{d}{L_0}$ in Fig. 13.

b) Third order Stokes' equations for $\frac{1}{25} < \frac{d}{L} < \frac{1}{2}$. This is a nonlinear theory. There are other Stokes' equations of higher order, but they generally do not improve the accuracy commensurate with the increased computations involved and so will not be discussed.

c) Cnoidal theory for $\frac{d}{L} < \frac{1}{25}$ --not made use of due to excessive computations being involved. Approximate results in this range may be obtained from the theory in b).

d) Solitary wave theory for breaking waves, broadly valid when $\frac{H}{d} \geq 0.78$. For a first check, the value of H given by deep water expressions may be used in checking this inequality.

In the above,

d = depth of water below the original water level

L = wave length

and L is obtained from the equation:

$$L = \frac{gT^2}{2\pi} \tanh \frac{2\pi d}{L} \text{ for case a)}$$

$$L = \frac{gT^2}{2\pi} \tanh \frac{2\pi d}{L} \left[1 + \left(\frac{\pi H}{L}\right)^2 \left(\frac{14+4 \cosh^2 \frac{4\pi d}{L}}{16 \sinh^4 \frac{2\pi d}{L}}\right)\right] \text{for case b)}$$

$$L = \infty \text{ for case d).} \qquad (3.6)$$

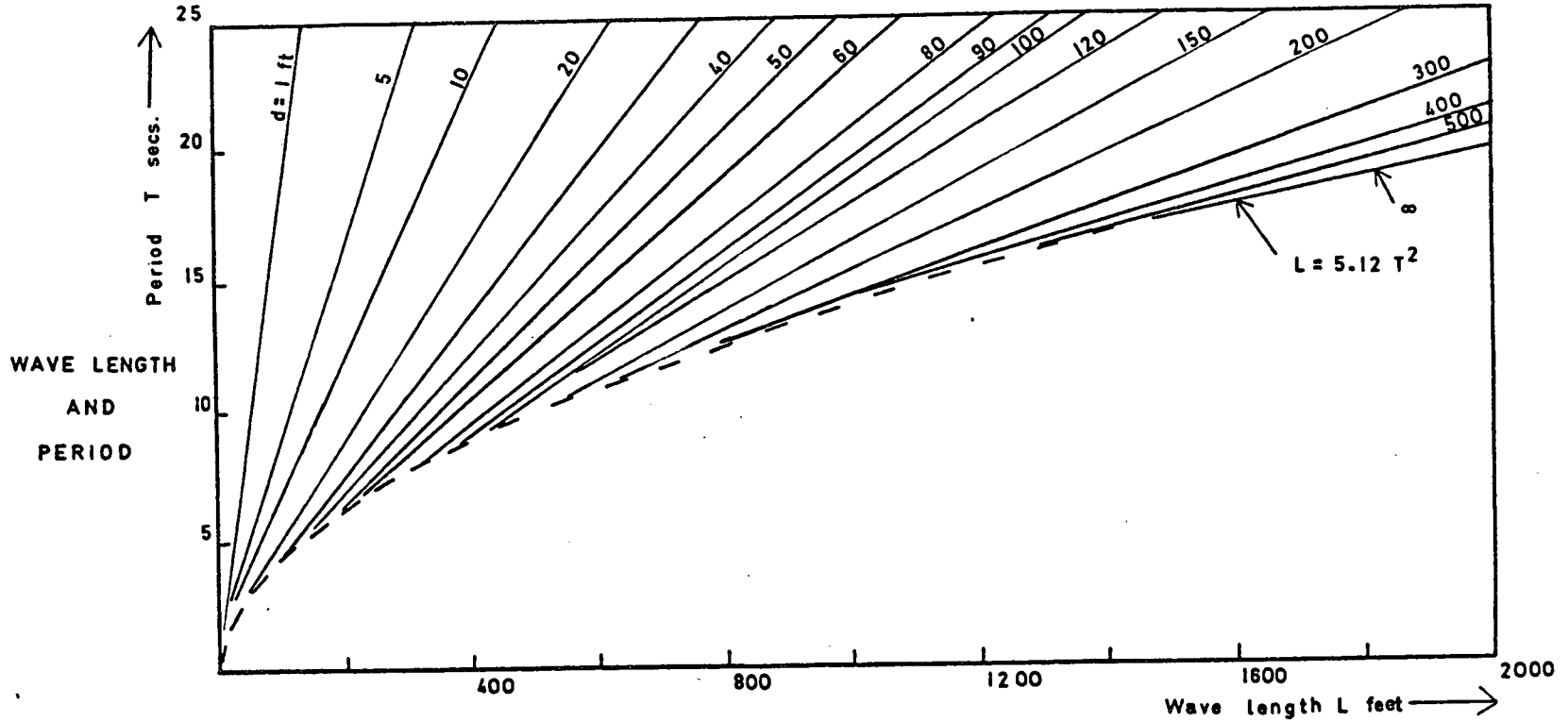
WAVE LENGTH
AND
PERIOD
Period T secs.
25
20
15
10
5
d = 1 ft
5
10
20
40
50
60
80
90
100
120
150
200
300
400
500
∞
L = 5.12 T²
400
800
1200
1600
2000
Wave length L feet

Fig 12

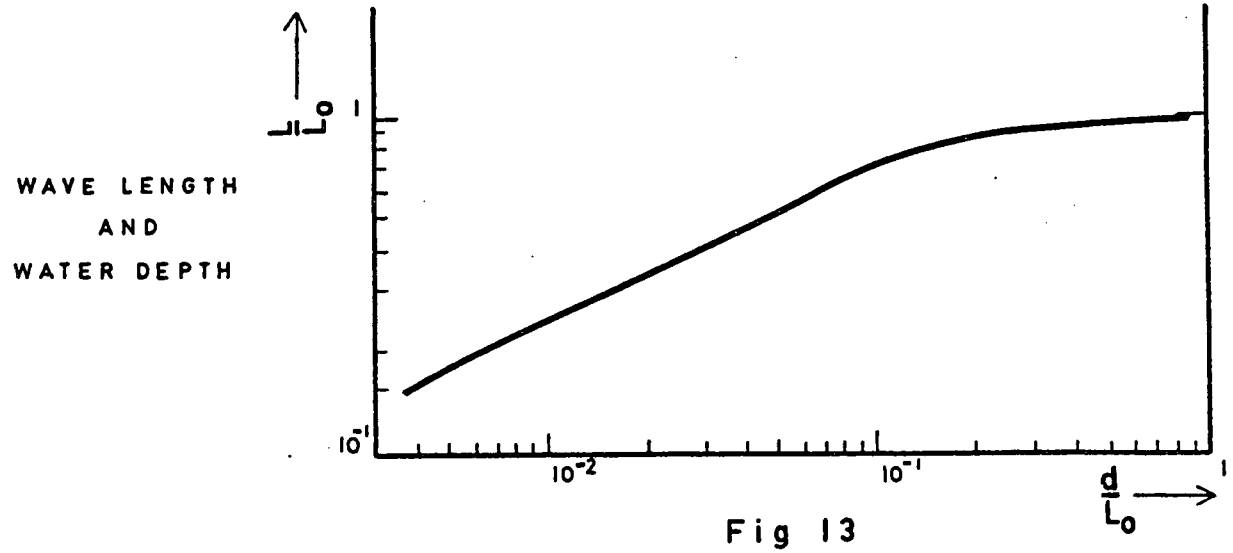
WAVE LENGTH
AND
WATER DEPTH
L/L₀
1
10⁻¹
10⁻²
10⁻¹
1
d/L₀

Fig 13

T = time period of the wave, with usual values < 16 secs. obtained as outlined in Section 3.2.

H is a variable selected as indicated in Section 3.2. For the limit of the range of the Cnoidal theory, namely $\frac{d}{L} = \frac{1}{25}$, a plot of the coefficient c in the following expression is given in Fig. 14:

$$L \text{ (Wave length in feet)} = cT^2$$

where T = wave period in seconds.

Appendix II gives a brief outline of the theories for a), b), c), and d). Only deterministic models of waves are considered.

In Table 3 the ranges of the relevant parameters over which the various wave theories are applicable have been indicated. A graphical representation of the ranges of validity of these theories is embodied in Fig. 15. The ranges pertinent to each theory are discussed in the succeeding paragraphs.

3.4 Characteristics of Stokes theory:

The mathematical basis for the Stokes shallow water (finite amplitude) and solitary wave theories are given in Appendix II.

The third order Stokes oscillatory shallow water theory gives a substantial improvement in accuracy over that in the small-amplitude theory mainly in the following ranges:

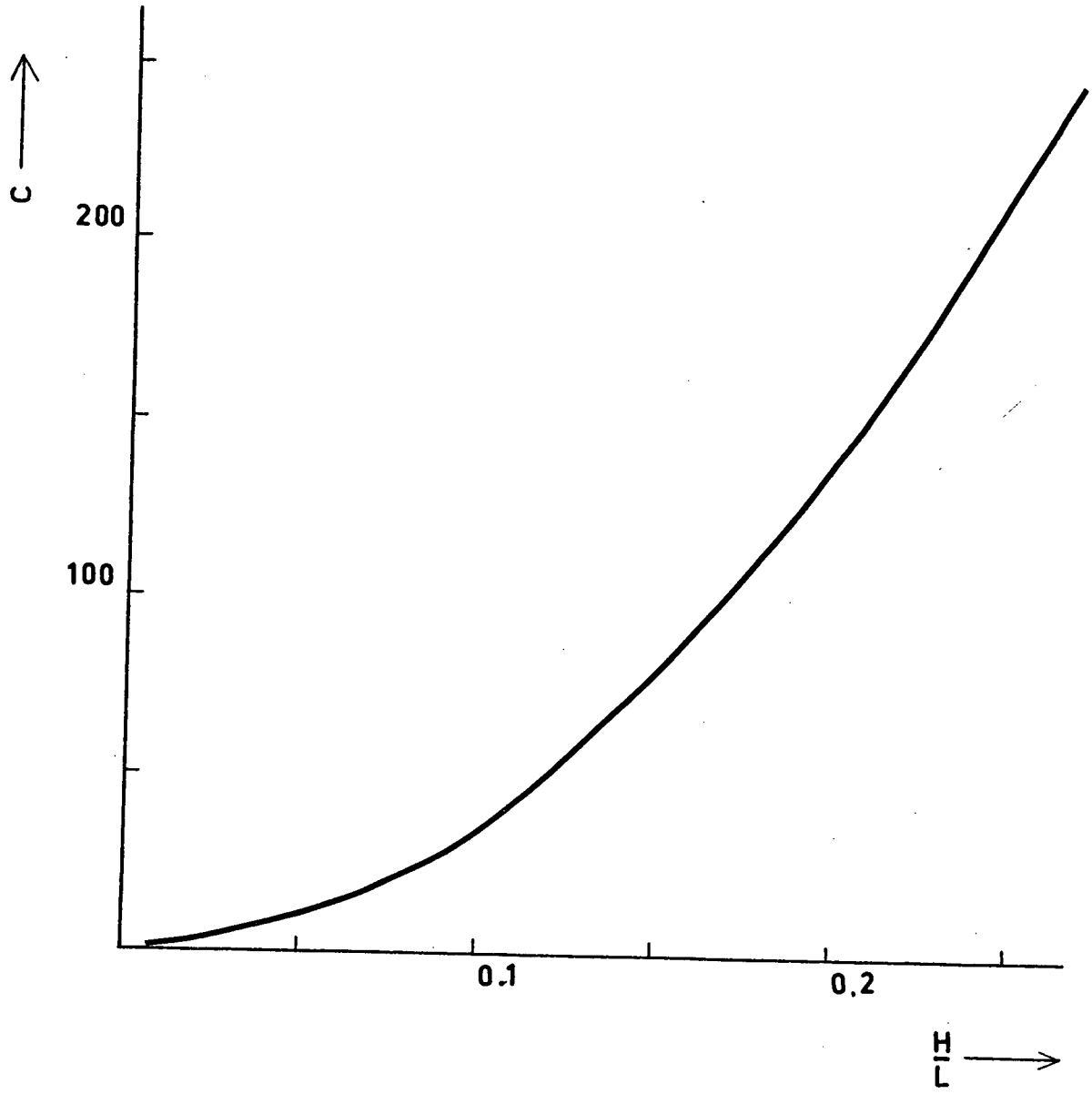


COEFFICIENT c

Fig 14

TABLE 3

RANGE OF APPLICABILITY OF THE WAVE THEORIES

| | Parameter | Linear Airy Theory | Stokes Shallow Water Finite-Amplitude | Cnoidal | Solitary Wave (Breaking) | No Theory-Interpolation |
|---|---|---|---|---|---|---|
| 1 | $\frac{d}{T^2}$ (ft./sec.$^2$) | $>2.5$ | $0.2<\frac{d}{T^2}<2.5$ | $<0.20$ | $<0.08$ | $0.08<\frac{d}{T^2}<2.5$ |
| 2 | Equivalent $\frac{d}{L}$ | $>0.5$ | $0.04<\frac{d}{L}<0.5$ | $<0.04$ | $<0.016$ | $0.016<\frac{d}{L}<0.5$ |
| 3 | $\frac{H}{T^2}$ (ft./sec.$^2$) | $<<0.3$ | $<0.3$ [limited range] | - | - ($\geq 9.8$) | Large $>0.3$ |
| 4 | Equivalent $\frac{H}{d}$ | v.small | - | $<0.78$ | $\doteq 0.78$ | $\frac{H}{d} < 0.78$ |
| 5 | Side condition for range of $\frac{H}{T^2}$ | - | - | - | $\frac{d}{T^2}<0.08$ | - |

N.B. 1. Figures are approximate.
2. Conditions 1,2,3 and 4 are taken together for classifying each case.

RANGES OF THEORIES

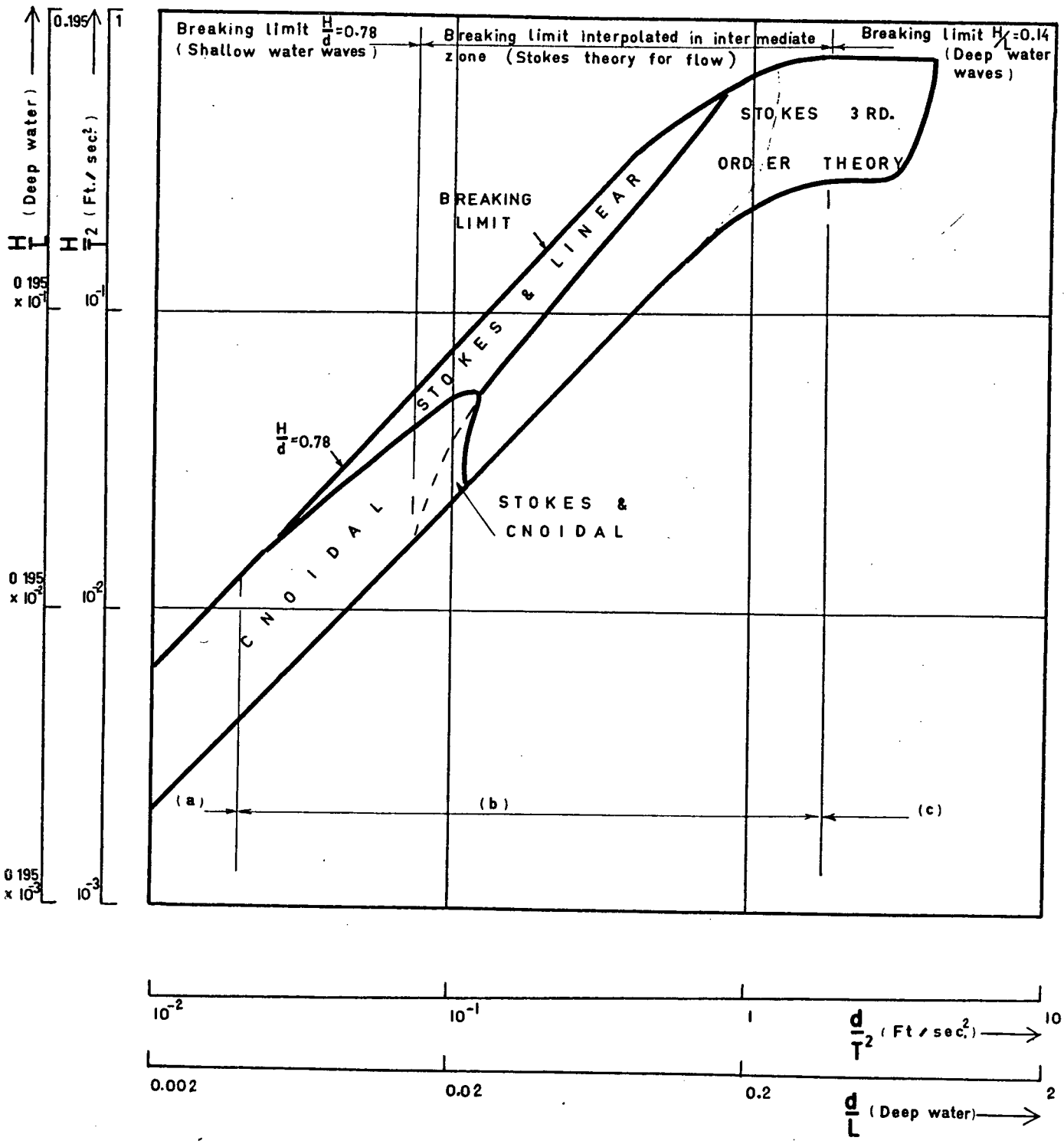


LEGEND

( a ) .. Breaking waves represented by solitary waves
( b) .. " " " " interpolated Stokes theory
( c ) .. " " " " deep water limit H/L = 0.142

Fig 15

$$\frac{d}{L} < \frac{1}{3} \text{ , i.e., } \frac{d}{T^2} < 1.8 \text{ ft./sec.}^2$$

or $$0.08 < \frac{H}{T^2} < 0.3 \text{ ft./sec.}^2$$

The most important expressions for the third order finite-amplitude theory, as summarised from Appendix II, are as follows:

$$\text{Wave velocity } C = \sqrt{\frac{gL}{2\pi}\tanh\frac{2\pi d}{L}\left[1+\left(\frac{\pi a}{L}\right)^2\left(\frac{14+4\cosh^2\frac{4\pi d}{L}}{16\sinh^4\frac{2\pi d}{L}}\right)\right]} \qquad (3.7)$$

$$\text{Wave length } L = \frac{gT^2}{2\pi}\tanh\frac{2\pi d}{L}\left[1+\left(\frac{2\pi a}{L}\right)^2\left(\frac{14+4\cosh^2\frac{4\pi d}{L}}{16\sinh^4\frac{2\pi d}{L}}\right)\right] \qquad (3.8)$$

$$\text{Wave height } H = 2a+\frac{2\pi^2}{L^2}a^3\left[\frac{3}{16}\left(\frac{1+8\cosh^6\frac{2\pi d}{L}}{\sinh^6\frac{2\pi d}{L}}\right)\right] \qquad (3.9)$$

$$\text{Depth of trough} = a \qquad (3.10)$$

$$\text{Horizontal velocity } u = C\left[F_1\cosh\frac{2\pi(z+d)}{L}\cos\left(\kappa x-\frac{2\pi}{T}t\right)+F_2\cosh\frac{4\pi(z+d)}{L}\cos 2\left(\kappa x-\frac{2\pi}{T}t\right)+F_3\cosh\frac{6\pi(z+d)}{L}\cos 3\left(\kappa x-\frac{2\pi}{T}t\right)\right] \qquad (3.11)$$

$$\text{Local acceleration } \frac{\partial u}{\partial t} = \frac{2\pi C}{T}\left[F_1\cosh\frac{2\pi(z+d)}{L}\sin\left(\kappa x-\frac{2\pi}{T}t\right)+2F_2\cosh\frac{4\pi(z+d)}{L}\sin 2\left(\kappa x-\frac{2\pi}{T}t\right)+3F_3\cosh\frac{6\pi(z+d)}{L}\cos 3\left(\kappa x-\frac{2\pi}{T}t\right)\right] \qquad (3.12)$$

$$\kappa = \frac{2\pi}{L} \qquad (3.13)$$

$F_1$, $F_2$ and $F_3$ = functions stipulated in Appendix II.

## 3.5 Additional limit (of wave steepness) of validity of third order Stokes' theory:

Apart from the following limit of the valid range (for transition to breaking waves in shallow water represented by the solitary wave theory), namely,

$$\frac{H}{d_b} \leq 0.75 \tag{3.14}$$

$d_b$ being the water depth below the trough, there is an additional limiting condition for the wave heights at which waves break. This is as under:

$$\frac{H}{L} = 0.142 \tanh \frac{2\pi d}{L} \tag{3.15}$$

(Linear deep water waves transform to breaking waves directly). For greater heights, the third order Stokes theory does not correctly represent the water kinematics.

For conditions intermediate between (3.14) and (3.15), values of breaking velocities are evaluated from wave heights and lengths obtained by interpolation. The Stokes shallow water wave theory is employed to compute particle velocities in such cases, the range of this modified approach being

$$\begin{aligned} 0.08 < \frac{d}{T^2} < 2.5 \text{ ft./sec.}^2 \\ 0.3 < \frac{H}{T^2} < 0.78 \text{ ft./sec.}^2 \end{aligned} \tag{3.16}$$

These limits apply to frictionless flat ocean beds.

The height of breaking waves would actually be considerably limited by the effect of the slope of the beach. Plots of experimental values of the breaker height H with its transformation along the bed inshore are available as guide-lines.[18,19] The plots are available as functions of $\frac{H}{L_0}$ , $\frac{H_0}{d}$ , and bed slope i

$H_0$ = wave height of incoming wave in deep water

$L_0$ = incoming wave length in deep water

d = water depth in shallow water.

3.6 Breaking waves:

Solitary wave theory:

This represents a symmetrical wave with the water surface almost wholly above the trough, as qualitatively shown in Fig. 16. The geometry of the wave is subject to the limit at Section 3.3 d', which applies to non-viscous flat ocean beds. For sloping beaches, the experimentally obtained values of modified variables such as H and d are available.[18,20] The relatively small reduction of breaking heights due to bottom friction is obtained from computation of the energy per wave cyele that is dissipated by laminar damping. This is obtained from the empirical expression

$$H = H_0 \, e^{(-\frac{\varepsilon_b x}{L})} \qquad (3.17)$$

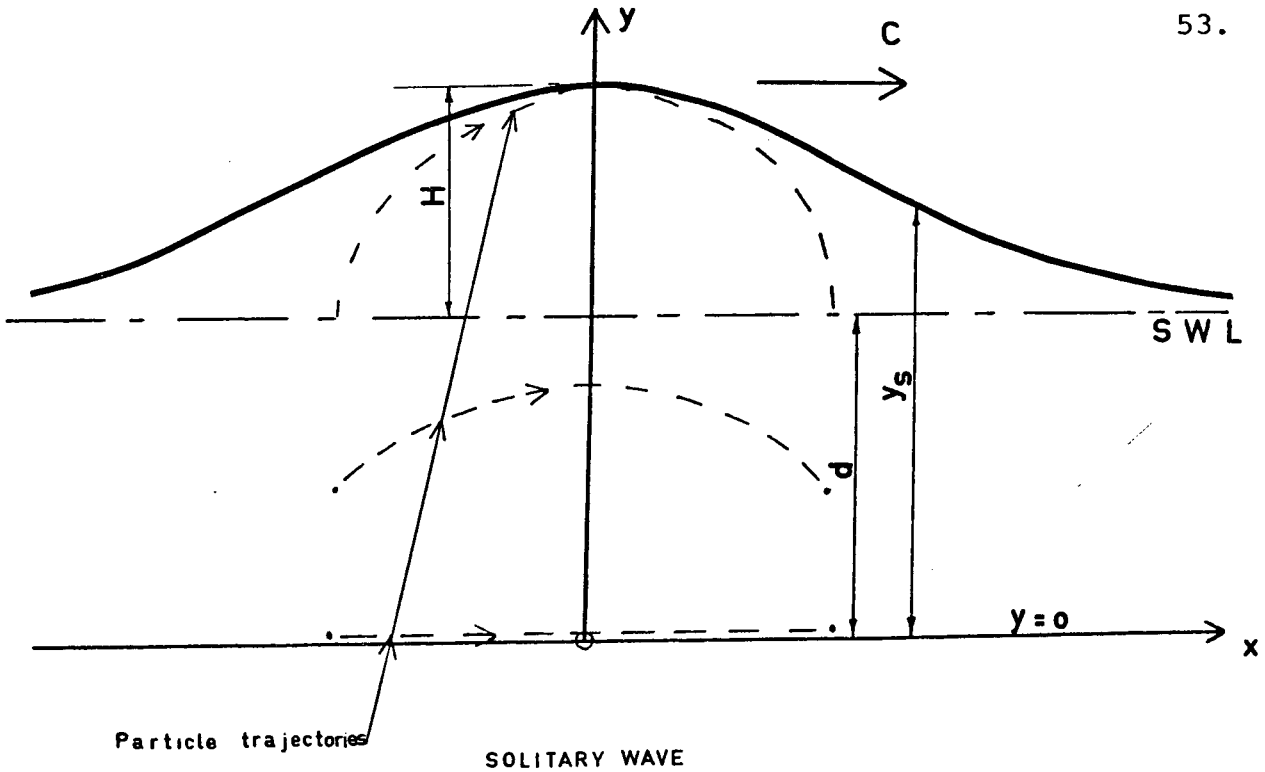


SOLITARY WAVE

Fig 16

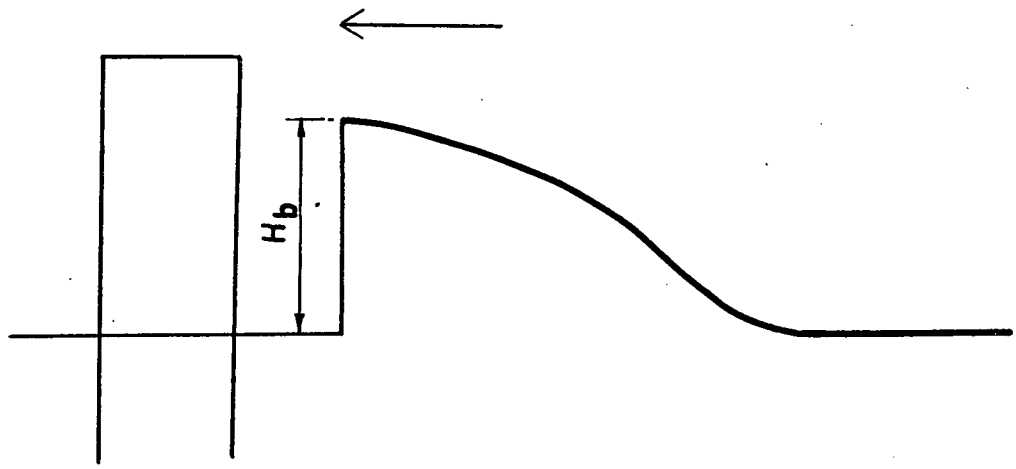


IMPACT

MODEL

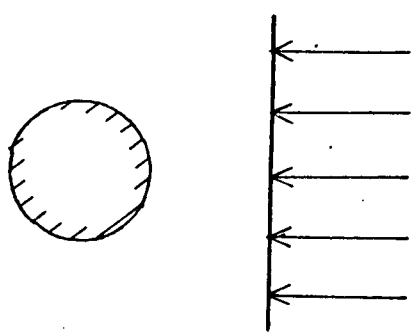

Fig 17

where $\varepsilon_b$ is a bottom damping factor which increases with increasing kinematic viscosity $\nu$.

$\varepsilon_b$ decreases with increasing water depths and wave length and increases with wave period. $\varepsilon_b$ takes on values from $10^{-3}$ to $2 \times 10^{-2}$.

x = distance from the toe of the beach slope.

These values for breaking wave heights are fed back into the solitary wave relations.

3.7 Impact type of breaker forces:

This model (Fig. 17) is accurate for asymmetric breaking wave profiles such as plunging waves and the steeper among the spilling waves. The impulse for each wave is obtained from drag expressions for piles. The portion of the impulse due to change of momentum on contact is comparatively small. In particular cases the computed impact-type excitations were found to be smaller than those for solitary wave representations.

3.8 Determinants of breakers:

Fig. 18 indicates 4 regions in the i - $\frac{H_0}{d}$ plane (i being the beach slope, $H_0$ the deep water wave height) when different types of waves reach the shore--spilling, plunging, and non-breaking.[7] The breaker heights exceeded the theoretical figure of 0.78d in model tests with appreciable bed slope. The plot at Fig. 18 demarcates breaking regimes from non-breaking ones. Plunging waves generate the highest velocities

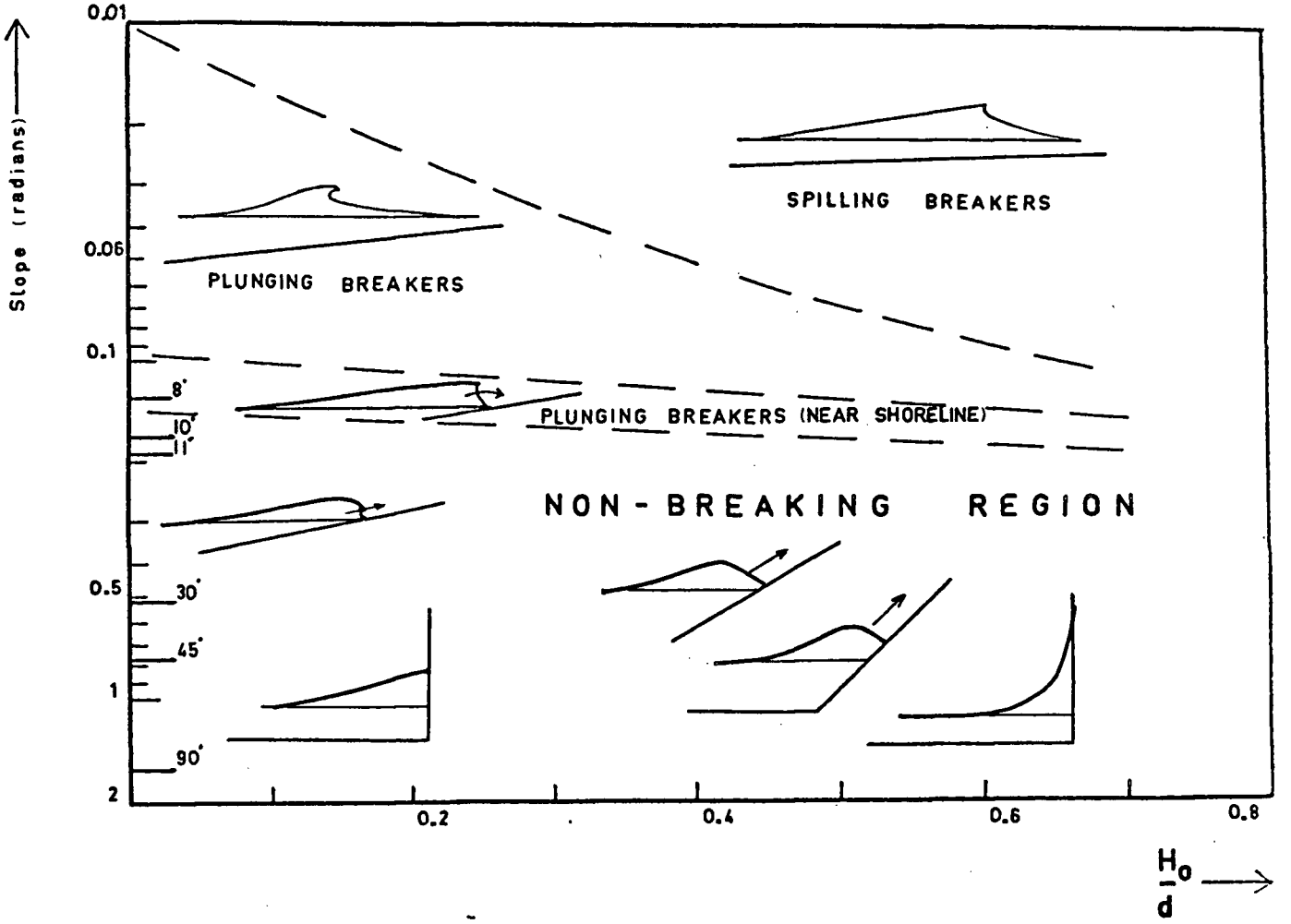
Slope (radians)
0.01
0.06
0.1
0.5
1
2
8°
10°
11°
30°
45°
90°
SPILLING BREAKERS
PLUNGING BREAKERS
PLUNGING BREAKERS (NEAR SHORELINE)
NON-BREAKING REGION
0.2
0.4
0.6
0.8
Ho/d
BREAKER RANGES

Fig 18

and wave forces out of the various types of breaking waves. The solitary wave model represents the plunging type of breaker fairly accurately and hence wave force calculations for the solitary wave, without any scaling, would be conservative for other breakers also.

3.9 Earthquake motion:

The primary input used in this thesis is the ground acceleration record of an actual earthquake. The dynamical problem is formulated in terms of the motion of the structure relative to the ground, the absolute motion of the structure being the superposition of the relative motion and the ground motion. Since the ground motion occurs without imparting any motion to the main body of the water, the absolute structure motion is also the relative structure--fluid motion (in the absence of other waves).

However the range of the total motion is such that it would not cause separation and vortex-shedding; therefore the values of $C_M$ and $C_D$ in the pre-separation range should be effective. This was checked by numerical computations for stiff as well as flexible structures.

3.10 Comparative ground accelerations:

The characteristics of the El Centro, 1940, N.-S. ground record and the Taft, July 21, 1952 S.21°W ground record, which were used as the inputs to the structures analysed, are

now stated. The El Centro ground motion persists strongly for the first 10 seconds and less perceptibly till the 30th second reaching a maximum acceleration of 0.3g at 2.5 sec. The dominant frequency is 2.05 cycles/sec. The Taft ground motion extends appreciably for 30 seconds and reaches a maximum acceleration of 0.144g at t = 4.1 secs. The dominant frequency is 3.0 cycles/sec.

# CHAPTER IV

## DYNAMIC RESPONSE PROBLEM

This chapter presents the systems of differential equations of motion for framed structures used to compute the dynamic response to the earthquake excitation and wave force inputs discussed in the previous chapters.

### 4.1 Origin of nonlinear terms:

The structural analysis portion is a linear damped dynamic problem using the standard stiffness method of formulation. Nonlinear terms are introduced through the forces applied to the structure which arise through the inertia and drag forces of the fluid on the structure due to the relative displacement.

### 4.2 Assumptions:

The following assumptions have been made in the dynamic formulation:

1) The framed structure is elastic, has cylindrical members and is symmetric normal to the direction of the ground/wave motion.
2) Rotatory and vertical translatory inertia are neglected, an assumption checked subsequently by computations.

3) Fluid forces and resistances can be discretised at nodes

4) The effect of the change of section shape on fluid-cylinder interaction was neglected

5) Fluid forces on the cylinder are two-dimensional in nature.

## 4.3 Basic formulation:

The basic equation for the dynamical problem is of the form

$$[m]\{\ddot{U}\} + [C_{str.}]\{\dot{U}\} + [k]\{U\} + \{H(\dot{U}_r, U_r)\} = P(t) \qquad (4.1)$$

where

$\{U\}$ = n x 1 vector of generalised coordinates, which in this case represents the reduced column matrix of horizontal nodal displacements.

$[m]$ = mass matrix.

$[C_{str}]$ = relative viscous damping matrix representing internal damping related to the reduced vector of velocities $\{\dot{U}\}$. The individual terms of the matrix are obtained[26] by setting constants $\alpha$ and $\beta$ in the expression

$$C_{ij} = \alpha\, m_{ij} + \beta\, k_{ij}$$

so that the percentage of critical damping in the first two modes is a preselected value.

[k] = reduced stiffness matrix with respect to horizontal translations only.

$\{H(\dot{U}_r, \ddot{U}_r)\}$ = vector of forces due to the hydrodynamic effect, which is a function of the relative velocities and accelerations between structure and fluid.

$\{P(t)\}$ = vector of other forces on the system. These forces may be either physical forces or conceptual forces such as the imparted inertia in the earthquake case. Dots represent time-differentiation.

4.4 Earthquake inputs:

The exact form of the equations of motion is established on the assumptions stated in Section 4.2. In matrix form the equations are written as:

$$[[m_s]+[K_m V]]\{\ddot{U}_r\}+[[m_s]+[K_m V]]\{\ddot{U}_g\}+[C_{str}]\{\dot{U}_r\}+[K_D A|(\dot{U}_r+\dot{U}_g)|]\{\dot{U}_r+\dot{U}_g\}$$

$$+[k]\{U_r\} = \{0\} \qquad (4.2)$$

An equivalent equation of dynamic equilibrium is

$$[[m_s]+[K_m V]]\{\ddot{U}\}+[C_{str}]\{\dot{U}\}+[K_D A|\dot{U}|]\{\dot{U}\}+[k]\{U\}$$

$$= [C_{str}]\{\dot{U}_g\}+[k]\{U_g\} \qquad (4.3)$$

where $\{U_r\}$ = n x 1 vector of generalised coordinates, i.e., displacements relative to the ground in the horizontal direction

$\{U_g\}$ = n x 1 vector of the ground displacement, a given function of time. Every element of the vector $\{U_g\}$ is the same function of time.

$\{U\}=\{U_r+U_g\}$ = vector of absolute displacements which was also that relative to water.

$[m_s]$ = diagonal matrix of discretised masses in the structure (off-diagonal terms appear in case of coupling)

$[K_m V]$ = diagonal matrix of added mass, containing the coefficient of mass, water density and the enclosed volume corresponding to each node.

$[K_D A(|\dot{U}+\dot{U}_g|)]\{\dot{U}+\dot{U}_g\}$ = n x 1 vector of fluid drag forces.

$[C_{str}]$ = as previously defined.

$[k]$ = as previously defined.

Dots represent time-differentiation.

4.5 Further simplifications:

Equation (4.3) represents a system of nonlinear differential equations with variable coefficients. To evaluate the importance of $C_M$ and $C_D$ in the overall response they were assumed to be constant at a particular value throughout the motion, with a separate computation being made for every different choice of $C_M$ and $C_D$. Assuming $C_M$ and $C_D$ as constants allows the equations of motion to be reduced to a system with constant coefficients as under:

$$[m_{virtual}]\{\ddot{U}_r+\ddot{U}_g\}+[C_{str}]\{\dot{U}_r\}+[K_D A(|\dot{U}_r+\dot{U}_g|)]\{\dot{U}_r+\dot{U}_g\}+[k]\{U_r\} = \{0\} \qquad (4.4)$$

or equivalently

$$[m_{virtual}]\{\ddot{U}\}+[C_{str}]\{\dot{U}\}+[K_D A|\dot{U}|]\{\dot{U}\}+[k]\{U\}$$

$$= [C_{str}]\{\dot{U}_g\}+[k]\{U_g\} \qquad (4.5)$$

where $[m_{virtual}]$ incorporates constant values of $K_m$.

4.6 Method of solution:

The equation (4.4) was solved by time-step numerical integration for specific ground motion record inputs. Previous studies have led to techniques for linearising the non-linear drag terms. For a deterministic input no advantage is thereby secured, since iterations are involved, and linearisation was not resorted to. The 3rd order Runge-Kutta method was used for numerical solution, and the formulae for this are given in Appendix III. The size of the time steps had to be kept down to 1/4 to 1/10 of the smallest of the natural periods of the structure in order to maintain stability of the solution. The steps ranged from 0.005 seconds to 0.0005 secs., the latter for structures with 10 degrees of freedom, and these were sufficiently small to follow the fluctuations in the irregular ground record. Chapter V details the structures analysed and the types of ground record used for input.

4.7 Wave force input:

Besides the assumptions in Section 4.2 it was necessary to simplify the excitation which though deterministic

in direction in shallow water, is stochastic with respect to amplitudes and frequency. A further assumption in the analysis of structures consisted in allowing for the contribution of only one set of sway-bracings to the stiffness, noting their large slenderness. Lift forces were assumed to be negligible and the flow presumed to be sub-critical. The equations of motion become:

$$[m_s]\{\ddot{U}\}+[C_{str}]\{\dot{U}\}+[k]\{U\}$$

$$= [K_m V]\{\dot{V}_W-\ddot{U}\}+[K_D A(|V_W-\dot{U}|)]\{V_W-\dot{U}\} \qquad (4.6)$$

where $\{V_W\}$ = vector of water particle velocities at the structure nodes,

and other symbols are as previously defined.

4.8 Wave response computations:

The larger of the wave heights give rise to high water particle velocities and resulting high drag forces. Then the equations of motion become highly nonlinear. They were solved by numerical time-step integration extending over several cycles until the amplitude in successive wave cycles converged to a steady-state value. While selecting the inputs for response computations, as elaborated in Chapter V, a period of the nonlinear wave resonant to the structural period and the greatest corresponding amplitude of excitation (i.e., wave height) in each case were chosen.

# CHAPTER V

## RESULTS OF COMPUTATIONS

Calculations of the dynamic response of selected structures to earthquake excitation and shallow water non-linear wave action are presented herein. Displacement response and stresses under the above two types of excitation along with those under breaking waves have been compared for selected structure geometries and water depths. The effect of varying the values of the parameters $C_M$ and $C_D$ on earthquake response has also been examined.

### 5.1 Choice of structures for evaluating earthquake response:

The structures chosen for analysis are diagrammatically shown in Fig. 19. Structures A and B have a resemblance to bell-type well-head structures and are totally submerged. The displaced volume is large for both A and B with the stiffness and natural frequency low for A. As the added masses are appreciable, the responses of A and B highlight the influence of $C_M$. Structure C represents the other extreme of the range of displaced volumes and structural stiffness. It is a tower-supported deck platform structure with a relatively small enclosed volume and a high natural frequency. The natural periods and mode shapes for the three

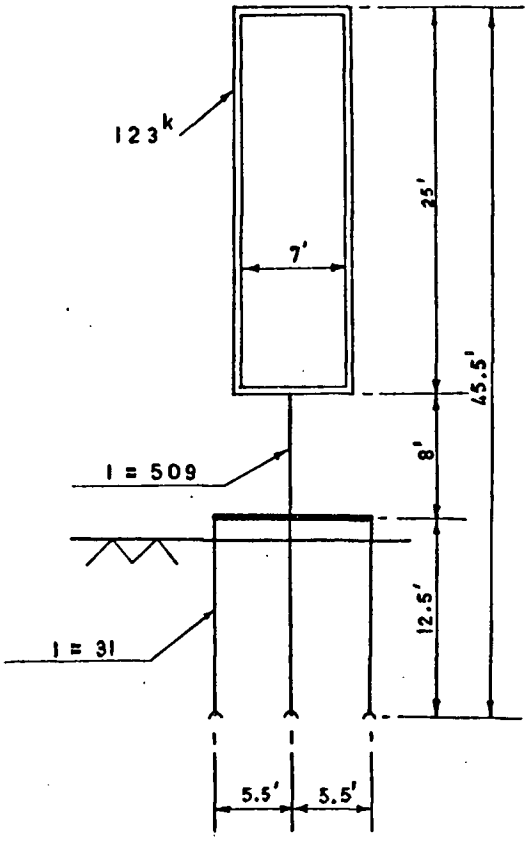


STRUCTURE A

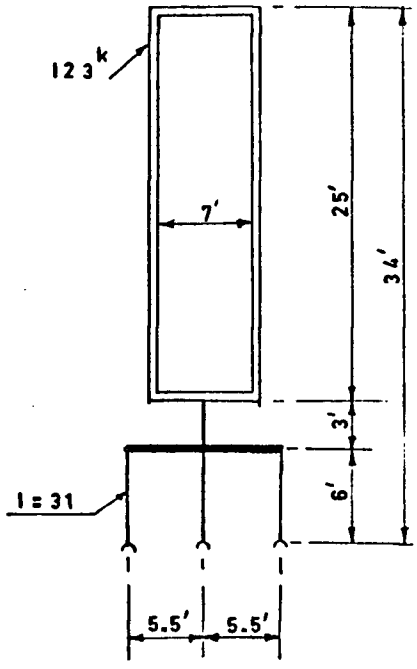


STRUCTURE B

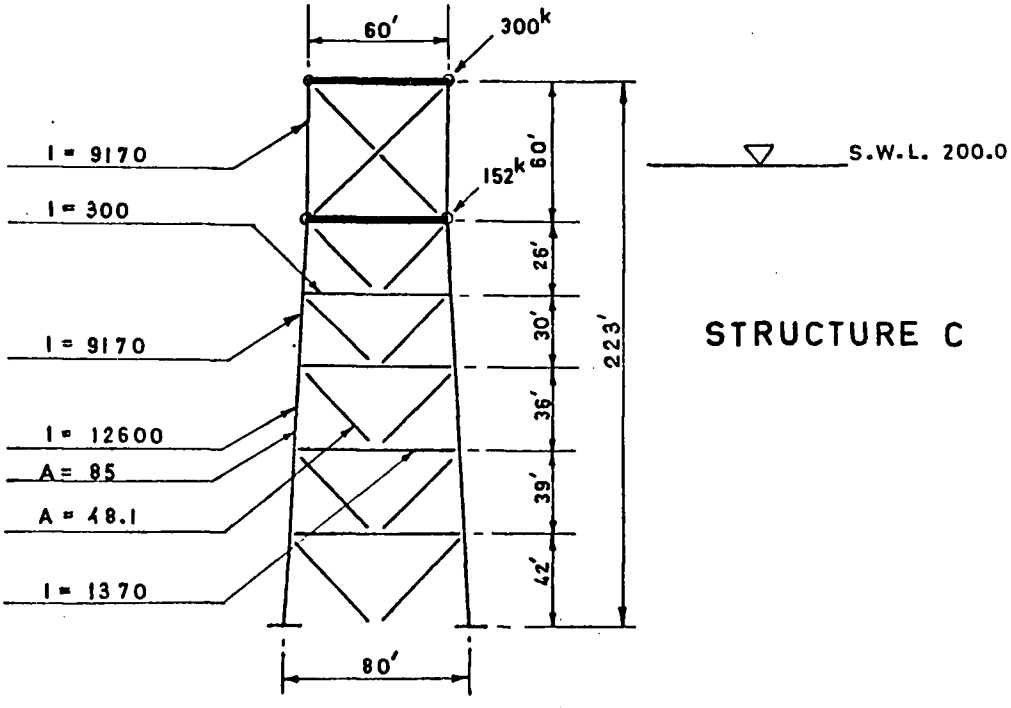


STRUCTURE C

Fig 19

structures are given in Table 4 where the nodes represent only horizontal degrees of freedom (as used in the reduced stiffness matrix) and are numbered as shown in Fig. 20. For the fully submerged bells A and B, it is seen that the influence of $C_M$ increases the fundamental period by as much as 25 percent. In arriving at the tabulated values of the periods and in calculations of the response, the distributed mass/inertia characteristics of the upper member of structures A and B were taken into account. Beam members of the plane frame type were used in modelling the structures, a member having six degrees of freedom.

5.2 Earthquake response:

The range of parameters $C_M$, $C_D$ and the percent critical (structural) damping for which computations were made, are given in Table 5. In addition to the El Centro ground shock which was applied to the three structures, the Taft ground record was also used as the input for structure A. The response-maximum displacements and base shears--to earthquake inputs for progressively increasing values of the parameter $C_M$ are tabulated in Table 6. For larger values of $C_M$, which cause longer fundamental periods, the maximum displacement under the El Centro input increased for structure A as expected (of the order of the following):

20% over the range $1.0 < C_M < 1.5$

6% over the range $1.5 < C_M < 2$

26% over the range $1 < C_M < 2$).

The maximum base shear for structure A also increased by about 42 percent as $C_M$ increased from 1 to 2. For structure B the

## KEY TO MODE SHAPES

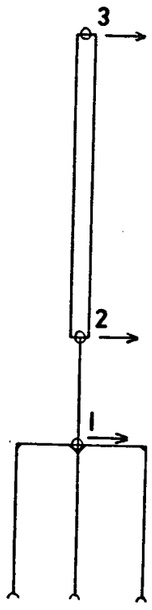


STRUCTURE A

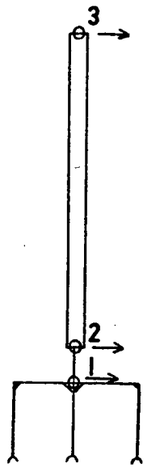


STRUCTURE B

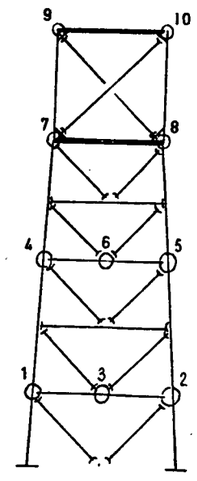


STRUCTURE C

Fig. 20

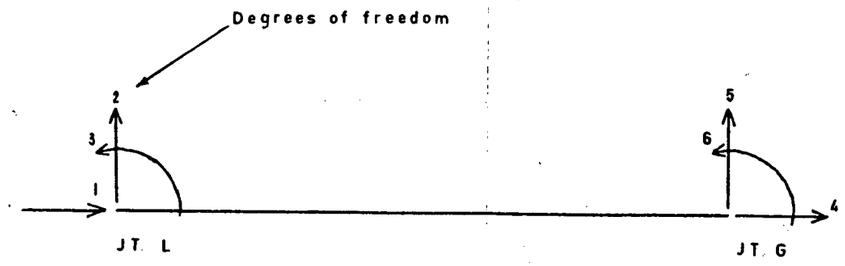


Shear deformations not considered

## PLANE BEAM ELEMENT

TABLE 4

PERIODS AND MODE SHAPES

| Structure | No. of Nodes | Mode | $C_M$ | Natural Periods (secs) | | Mode Shape | | | Participation Factor (For Linear Behaviour) |
|---|---|---|---|---|---|---|---|---|---|
| A | 3 | 1 | 1+0 | 2.3 | Node | 1 | 2 | 3 | 1.485 |
| | | | | | Ampl. | 0.129 | 0.259 | 0.957 | |
| | | 1 | 1+1 | 2.814 | | 1 | 2 | 3 | 1.49 |
| | | | | | | 0.129 | 0.259 | 0.957 | |
| | | 2 | 1+0 | 0.383 | | 1 | 2 | 3 | 1.010 |
| | | | | | | -0.691 | -0.593 | 0.412 | |
| | | 2 | 1+1 | 0.463 | | 1 | 2 | 3 | 1.04 |
| | | | | | | -0.992 | -0.595 | 0.411 | |
| | | 3 | 1+0 | 0.038 | | 1 | 2 | 3 | 0.080 |
| | | | | | | 0.992 | -0.110 | 0.066 | |
| | | 3 | 1+1 | 0.042 | | 1 | 2 | 3 | 0.077 |
| | | | | | | 0.994 | -0.090 | 0.054 | |
| B | 3 | 1 | 1+0 | 1.217 | | 1 | 2 | 3 | 1.488 |
| | | | | | | 0.067 | 0.129 | 0.989 | |
| | | 1 | 1+1 | 1.49 | | 1 | 2 | 3 | 1.495 |
| | | | | | | 0.067 | 0.129 | 0.989 | |
| | | 2 | 1+0 | 0.153 | | 1 | 2 | 3 | 1.234 |
| | | | | | | -0.660 | -0.646 | 0.385 | |
| | | 2 | 1+1 | 0.186 | | 1 | 2 | 3 | 1.255 |
| | | | | | | -0.660 | -0.646 | 0.384 | |
| | | 3 | 1+0 | 0.008 | | 1 | 2 | 3 | 0.0805 |
| | | | | | | 0.997 | -0.068 | 0.037 | |
| | | 3 | 1+1 | 0.009 | | 1 | 2 | 3 | 0.078 |
| | | | | | | 0.998 | -0.054 | 0.029 | |

TABLE 4 (Cont'd.)

| Structure | No. of Nodes | Mode | $C_M$ | Natural Period (secs) | Mode Shape | Participation Factor (For Linear Behaviour) |
|---|---|---|---|---|---|---|
| C | 10 | 1 | 1+1 | 0.99 | Node 1&2* 3 4&5* 6 7&8* 9&10*<br>Ampl. 0.128 0.145 0.475 0.490 0.78 1.0<br>Anti-symmetric mode | 1.192 |
| | | 2 | 1+1 | 0.263 | 1&2 3 4&5 6 7&8 9&10<br>0.525 0.594 1.0 0.772 0.27 -0.387<br>Anti-symmetric mode | 0.636 |
| | | 3 | 1+1 | 0.145 | 1&2 3 4&5 6 7&8 9&10<br>1.0 0.909 -0.345 -0.368 -0.313 0.135<br>Anti-symmetric mode | 0.503 |
| | | 4 | 1+1 | 0.114 | 1&2 3 4&5 6 7&8 9&10<br>0.17 0.134 -0.518 -0.313 1.0 -0.249<br>Anti-symmetric mode | 0.056 |
| | | 5 | 1+1 | 0.078 | 1&2 3 4&5 6 7&8 9&10<br>0.088 0 -1.0 0 0.003 0<br>Anti-symmetric mode | 0.0005 |
| | | 6 | 1+1 | 0.075 | Symmetric mode | 0.0005 |
| | | 7 | 1+1 | 0.039 | Symmetric mode | 0.0002 |
| | | 8 | 1+1 | 0.036 | Symmetric mode | 0.0002 |
| | | 9 | 1+1 | 0.023 | Anti-symmetric mode | 0.016 |
| | | 10 | 1+1 | 0.017 | Anti-symmetric mode | 0.001 |

*Ampls. equal in anti-symmetric modes, but equal and opposite in symmetric modes.

TABLE 5

RANGE OF PARAMETERS

| Structure | $C_M$ | $C_D$ | % Critical Damping | T (secs.) A | T (secs.) B |
|---|---|---|---|---|---|
| A } | 1+1 | 1.2 | 2 | 2.81 | 1.49 |
| B } | 1+0.75 | 1.2 | 2 | 2.68 | 1.42 |
| (For El Centro) | 1+0.5 | 1.2 | 2 | 2.56 | 1.35 |
| | 1+0 | 1.2 | 2 | 2.3 | 1.22 |
| | 1+1 | 0 | 2.5 | 2.81 | 1.49 |
| | 1+1 | 0 | 3 | 2.81 | 1.49 |
| | 1+1 | 0 | 4 | 2.81 | 1.49 |
| | 1+1 | 0 | 5 (A only) | 2.81 | - |
| C | 1+1 | 1.2 | 2 | 0.99 | |
| (For El Centro) | 1+0 | 1.2 | 2 | 0.988 | |
| A | 1+1 | 1.2 | 2 | 2.81 | |
| (For Taft) | 1+0.5 | 1.2 | 2 | 2.56 | |
| | 1+1 | 0 | 3 | 2.81 | |
| | 1+1 | 0 | 4 | 2.81 | |

N.B. $C_M$ = 1+0 indicates structure without water.

TABLE 6

EARTHQUAKE RESPONSE

| STR. | Earthquake Record | Parameters $C_M$ | Parameters $C_D$ | Parameters Ratio of Critical Damping $\zeta$ | Natural Period (secs.) | Maximum Displacement (ins.) | Maximum Base Shear (Kips) |
|---|---|---|---|---|---|---|---|
| A | El Centro 1940 | 1+0 | 1.2 | 0.02 | 2.30 | 17.95 | 28.91 |
| | | 1+0.5 | 1.2 | 0.02 | 2.56 | 21.42 | 36.12 |
| | | 1+0.75 | 1.2 | 0.02 | 2.68 | 22.51 | 37.91 |
| | | 1+1 | 1.2 | 0.02 | 2.81 | 22.60 | 51.2 |
| B | El Centro 1940 | 1+0 | 1.2 | 0.02 | 1.22 | 6.44 | 36.10 |
| | | 1+0.5 | 1.2 | 0.02 | 1.35 | 6.26 | 41.84 |
| | | 1+0.75 | 1.2 | 0.02 | 1.42 | 6.81 | 46.25 |
| | | 1+1 | 1.2 | 0.02 | 1.49 | 7.32 | 48.70 |
| A | Taft,1952 | 1+0 | 1.2 | 0.02 | 2.30 | 3.79 | 9.92 |
| | | 1+0.5 | 1.2 | 0.02 | 2.56 | 3.92 | 11.57 |
| | | 1+1 | 1.2 | 0.02 | 2.81 | 4.22 | 14.18 |
| C | El Centro, 1940 | 1+0 | 1.2 | 0.02 | 0.988 | 6.78 | 603.9 |
| | | 1+1 | 1.2 | 0.02 | 0.99 | 6.71 | 641.5 |

N.B. $C_M$ = 1+0 represents structure without water.

response was less sensitive to $C_M$. The percent increases over the range $1 < C_M < 2$ were 14 percent and 35 percent for displacement and shear respectively. In the case of structure C there was negligible difference in the response with or without the added mass effect. Constant values of

$$C_D = 1.2 \quad \text{and}$$

Percent critical damping $\zeta$ = 2 percent

were assumed in making the comparisons.

5.3 Effect of structural shape:

The effect of structural shape, i.e., displaced volume, stiffness and mass distribution on the response is illustrated by the three examples chosen. The smaller the displaced volume and the smaller the natural period, the less sensitive is the response to hydrodynamic effects.

5.4 Effect of $C_D$:

A similar parametric study varying $C_D$ showed that the response is insensitive to $C_D$ for earthquake inputs. Computations of the response for structure A with the nonlinear drag term and with that term being replaced by an additional equivalent viscous damping ratio of 0.01, 0.02 and 0.03 are given in Table 7. Comparing the maximum response in either case, additional damping effects due to water drag do not evidently exceed 2 to 3 percent critical viscous damping for such structures. Furthermore, for large-diameter cylinders, from Table 8, drag (and also

TABLE 7

DAMPING EQUIVALENT OF DRAG

| STR. | Earthquake Record | $C_M$ | $C_D$ | Ratio of Critical Damping $\zeta$ | Natural Period (secs.) | Maximum Displacement (ins.) | Maximum Base Shear (Kips) |
|---|---|---|---|---|---|---|---|
| A | El Centro, 1940 | 1+1 | 1.2 | 0.02 | 2.81 | 22.60 | 51.21 |
| | | 1+1 | 0 | 0.025 | 2.81 | 26.04 | 58.74 |
| | | 1+1 | 0 | 0.03 | 2.81 | 25.32 | 55.06 |
| | | 1+1 | 0 | 0.04 | 2.81 | 23.95 | 48.88 |
| | | 1+1 | 0 | 0.05 | 2.81 | 22.70 | 44.23 |
| A | Taft, 1952 | 1+1 | 1.2 | 0.02 | 2.81 | 4.22 | 14.18 |
| | | 1+1 | 0 | 0.03 | 2.81 | 4.13 | 13.39 |
| | | 1+1 | 0 | 0.04 | 2.81 | 4.00 | 12.25 |

TABLE 8

WATER INERTIA AND DRAG FORCES FOR STRUCTURE B

$T = 1.49 \quad C_M = 1+1 \quad C_D = 1.2$

El Centro Ground Record

| Node | | 1 | 2 | 3 |
|---|---|---|---|---|
| Ratio | $\frac{\text{(Max. Water Inertia Force)}}{\text{(Max. Drag Force)}}$ | 853.0 | 67.0 | 13.7 |

lift) effects are seen to be small compared with added inertia.

5.5 Relevance of subcritical region:

Checks of the instantaneous $N_R$ showed that except for very short durations at the extreme top node, the relative motion between fluid and structure was in the subcritical region. Further, flow separation would occur at only the topmost node of only the most flexible structures.

5.6 Dynamic response to finite-amplitude Stokes waves:

The results for a single pile (period 4.4 secs.) as well as 6 other pile-supported platforms of fundamental periods between 2.11 and 3.45 seconds are reported. The structures range in depth from 40 ft. to 100 ft., i.e., where shallow-water wave conditions would be encountered. While the structural configurations as shown in Fig. 21 are reasonably standard and amenable to practical construction, the member sizes and consequently the structural periods were chosen so as to induce resonance with ocean waves covering a practical range. The member sizes were therefore designed to keep the flexibility and natural periods high (over 2 secs.).

The values of the parameters $C_M$ and $C_D$ used, some of the structural sizes and selected wave data for which vibration response was computed are given in Table 9. The wave periods and heights were selected so that one of the harmonics of the

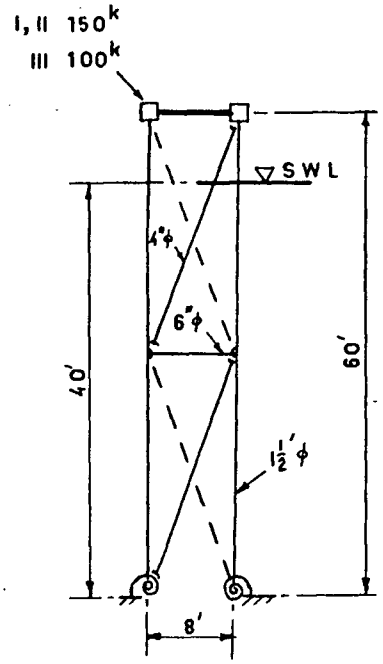


3 STRUCTURES
I, II & III

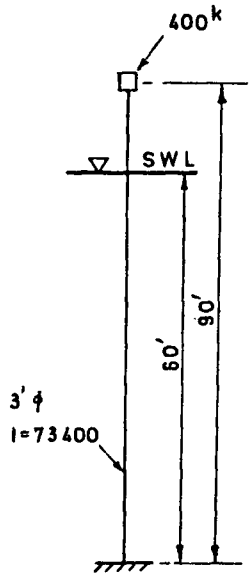


STRUCTURE IV

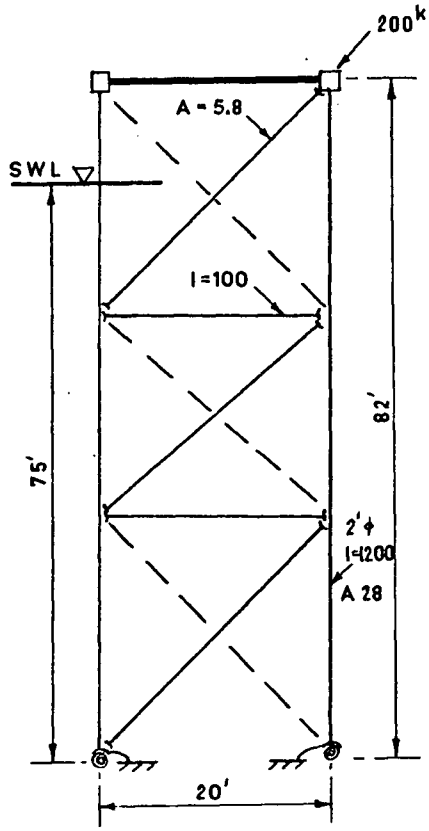


STRUCTURE V

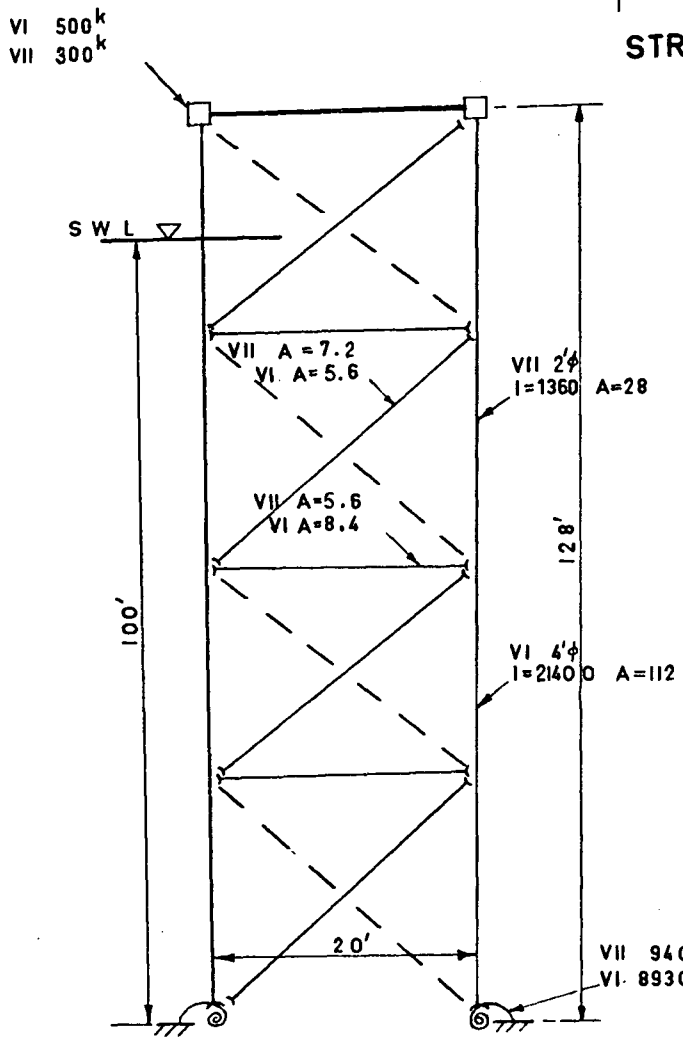


2 STRUCTURES VI & VII

STRUCTURES ANALYSED FOR WAVES

Fig 21

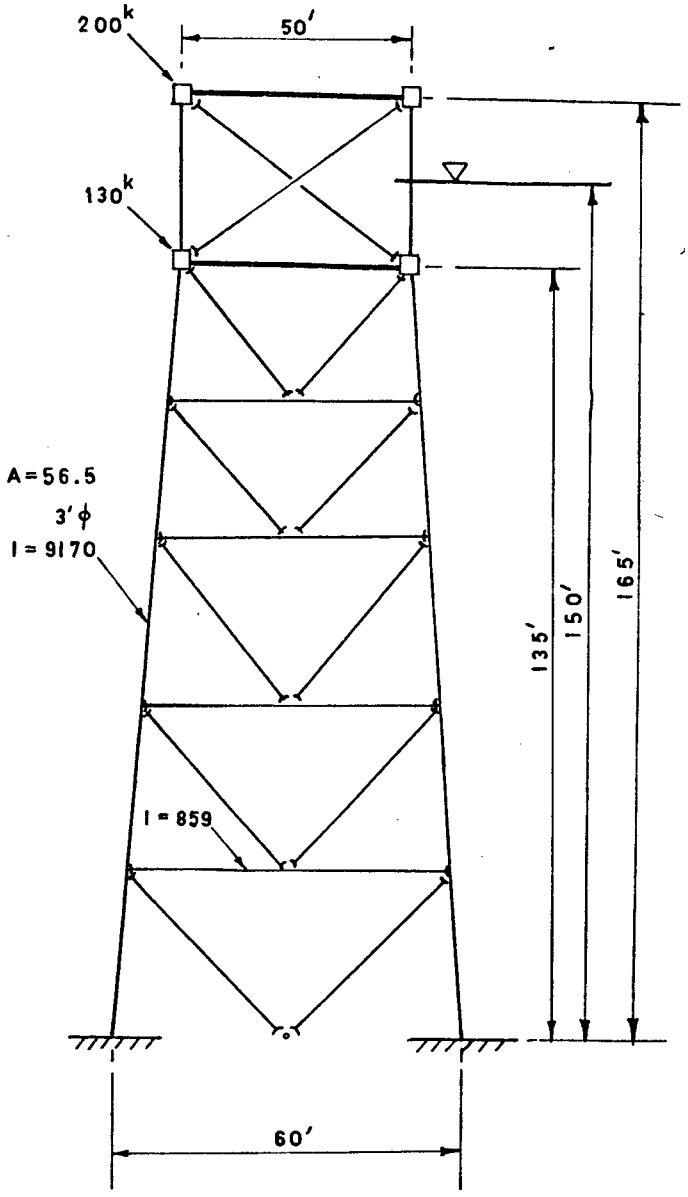


STRUCTURE X

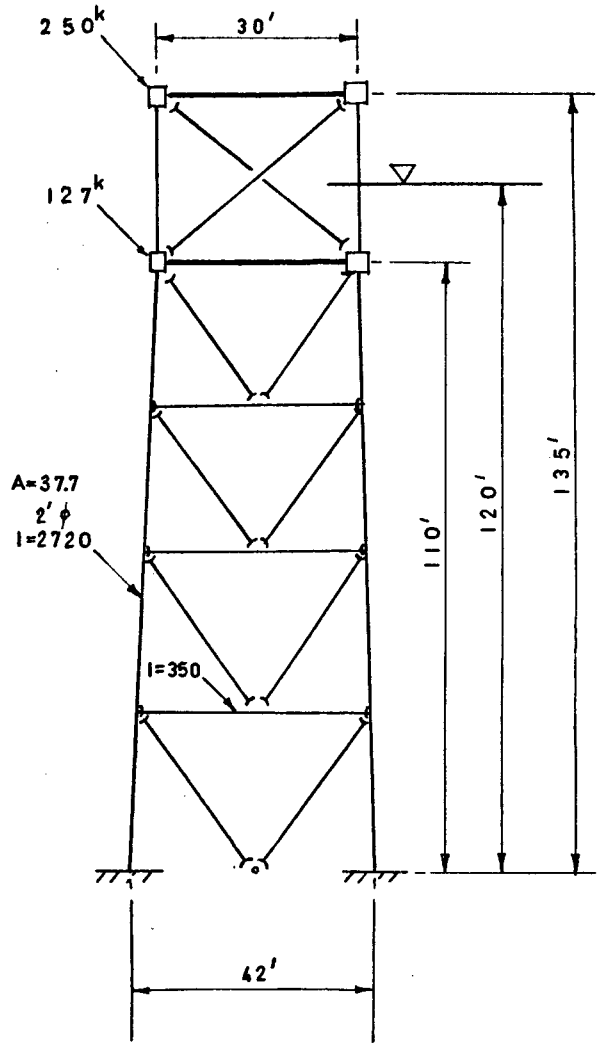


STRUCTURE IX

For Structure VIII, see Str. C of Fig 19

STRUCTURES ANALYSED FOR BREAKERS

Fig 22

TABLE 9

STRUCTURAL AND OTHER PARAMETERS FOR FINITE-AMPLITUDE WAVE RESPONSE

| Str. No. | Natural Period of Structure (secs.) 1st Mode | 2nd Mode | Base Fixity | Height of Structure Ft. | Dia. of Main Piles D Ft. | Total Projected Area Sq.Ft. | Total Enclosed Volume Cub.ft. | Ratio $\frac{\text{(Proj.Area)}}{\text{Enclosed Vol.}}$ Ft.$^{-1}$ | Depth of Water d Ft. | Period of Wave T sec. | Height of Wave H Ft. | Wave Length L Ft. | $\frac{d}{L}$ |
|---|---|---|---|---|---|---|---|---|---|---|---|---|---|
| I | 2.11 | 0.23 | Restrained $k=\frac{EI}{L}$ | 60 | 1.5 | 179.6 | 167 | 1.07 | 40 | 4.2 | 12 | 90 | .44 |
| II | 2.65 | 0.28 | Restrained $k=\frac{EI}{4L}$ | 60 | 1.5 | 179.4 | 155.2 | 1.16 | 40 | 5.3 | 19 | 139 | .29 |
| III | 3.45 | 0.40 | Fixed | 60 | 1.5 | 166.2 | 161.8 | 1.03 | 40 | 6.9 | 25 | 244 | .16 |
| IV | 4.4 | 0.50 | Fixed | 90 | 3 | 405 | 954.2 | 0.42 | 60 | 6.0 | 25 | 184 | .33 |
| V | 1.44 | 0.17 | Restrained $k=\frac{EI}{3L}$ | 82 | 2 | 336 | 490 | 0.69 | 75 | 2.87 | 5.8 | 42 | 1.79 |
| VI | 2.55 | 0.52 | Restrained $k=\frac{EI}{2L}$ | 128 | 4 | 997.6 | 2466 | 0.41 | 100 | 5.0 | 17 | 128 | .78 |
| VII | 2.84 | 0.41 | Restrained $k=\frac{EI}{L}$ | 128 | 2 | 467.6 | 612.8 | 0.75 | 100 | 5.65 | 21 | 164 | .61 |

k = rotational stiffness of base joint.

$C_D = 1.2$; $C_M = 2.0$

I,L are member inertia and length to next jt. for bottom section of pile.

nonlinear waves would be in resonance with the first mode of vibration of the structure. This criterion can be satisfied by matching the first harmonic of a small wave, with a correspondingly small energy input, or one of the higher harmonics of larger waves. The particular situations which generate the largest dynamic forces under the action of non-breaking waves are the ones reported here. Computations for breaking waves in these depths are presented later.

5.7 Computed response to Stokes waves:

Table 10 lists the maximum steady-state displacements and overturning moments at the base. Despite the fact that the period of the second harmonic of the wave excitation equalled the fundamental period in every case except Str. IV, the maximum displacements in Table 10 do not increase in a regular manner with increasing height d or such other parameter. A small change in structural period, as between I and II, causes a large change in dynamic response. Although the water depths are the same for I and II, the value of T selected to synchronise the second harmonic with structure II was greater; accordingly the wave size was greater, causing an increase in the ratio $\frac{H}{d}$. Consequently because of the comparatively greater amplitude of the second harmonic of the wave, the peak displacement is much greater for Str. II than for Str. I. The cases of structures VI and VII are similar.

TABLE 10

RESPONSE VALUES FOR FINITE-AMPLITUDE WAVE INPUT

| Str. | $T_n$ sec. | D Ft. | Ratio $\frac{\text{Projected Area}}{\text{Enclosed Volume}}$ $\text{Ft.}^{-1}$ | d Ft. | T Sec. | H Ft. | Max. Displacement $X_{max.}$ In. | Max. Displacement (Time After Crest) / (Wave Period) | Max. Overturning Moment K.In. |
|---|---|---|---|---|---|---|---|---|---|
| I | 2.11 | 1.5 | 1.07 | 40 | 4.2 | 12 | 4.63 | 0.4 | 24100 |
| II | 2.65 | 1.5 | 1.16 | 40 | 5.3 | 19 | 16.3 | 0.1 | 53200 |
| III | 3.45 | 1.5 | 1.03 | 40 | 6.9 | 25 | 41† | 0.2 | 82100 |
| IV | 4.4* | 3 | 0.42 | 60 | 6.0 | 25 | 28† | 0.4 | 38700 |
| V | 1.44 | 2 | 0.69 | 75 | 2.87 | 5.8 | 1.25 | 0.5 | 38500 |
| VI | 2.55 | 4 | 0.41 | 100 | 5.0 | 17 | 3.8 | 0.4 | 152000 |
| VII | 2.84 | 2 | 0.75 | 100 | 5.65 | 21 | 6.7 | 0.1 | 148600 |

N.B. $C_D = 1.2$

*Simple pile
†Flexibility high, nonlinear analysis warranted.

Other causes for the variations in maximum displacements are:

a) Greater wave heights H selected to accompany the greater T directly increases the amplitude of the excitation. This accounts for the comparatively high displacements for Str. II, III and VII.

b) The small area exposed to drag is seen to keep down the displacements for VI.

c) The extremely low structural stiffness of Str. III would engender a large "static deflection" and results in the large peak displacement shown.

d) The effective hydrodynamic damping ratio, a function of the average particle velocity, differs widely and influences resonance amplification.

Similarly the maximum overturning moments do not increase monotonically with either water depth or input wave height; nor do they increase in the same manner as the peak displacements. This is partly due to the fact that in different structures the degree of participation by the second mode varies.

5.8 Force variations with time:

A plot of the total wave force on the piles of a typical structure (Str. I) taking into account the motion of the structure is shown in Fig. 23. The total force from the variable water surface to the base of the pile has been plotted.

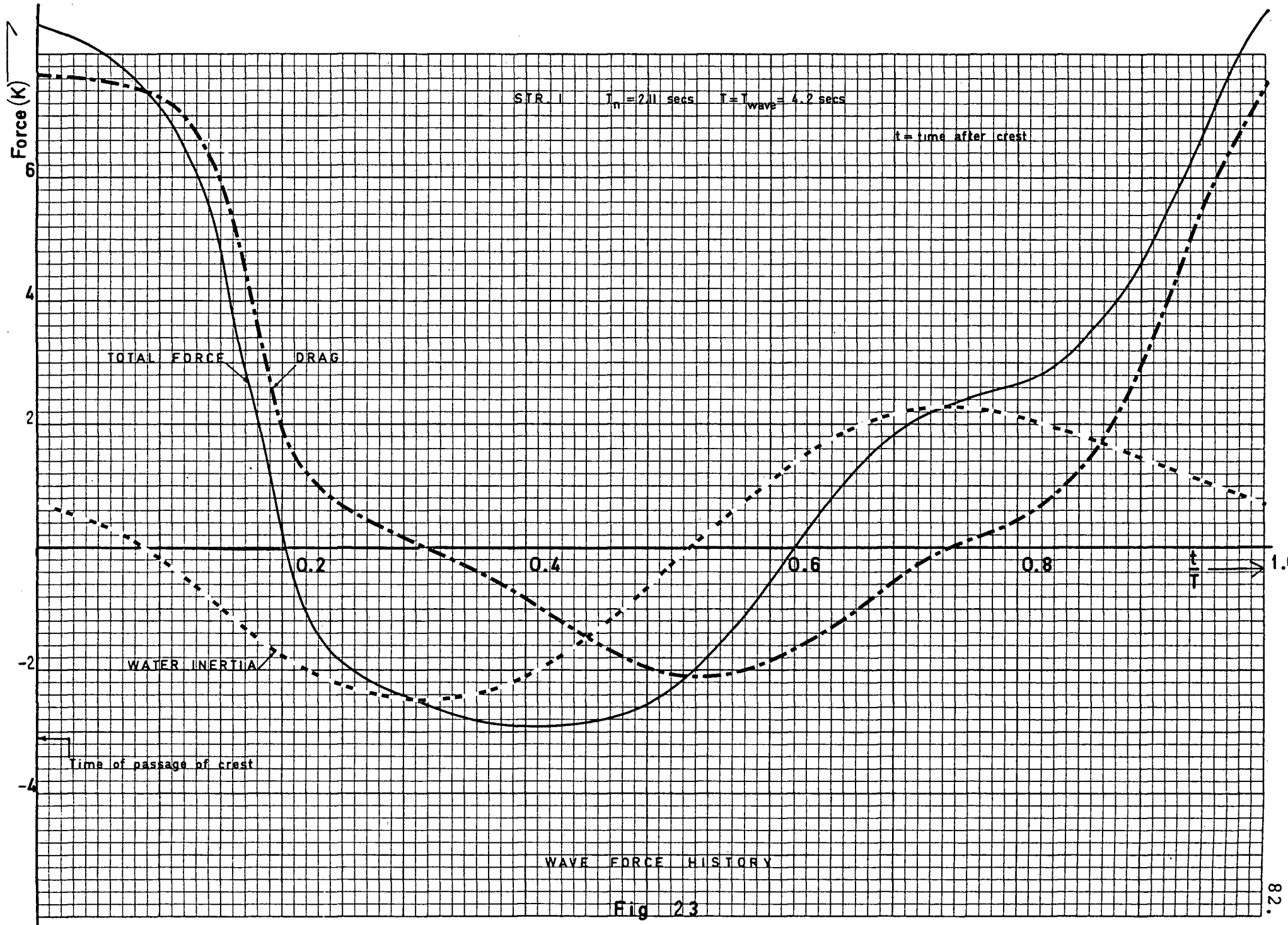


WAVE FORCE HISTORY

Fig 23

The plot indicates the following:

1) drag predominates over inertia for the structure in question, where the wave dimensions are large relative to the water depth.
2) the force-history plot is not symmetrical about the time of passage of the crest. This is due to the inertia force being at 90° phase and also to the change in the drag pattern owing to structure motion and higher order terms.
3) the inertia force plot is not symmetrical about the still water level time, this being due to higher order terms.

The time variation of the steady-state bending moment in the pile section adjacent to the platform for structure I is plotted in Fig. 24. The moment fluctuates at twice the frequency of the wave, which is explained by the fact that the second harmonic at half the wave period coincided with the structural period.

5.9 Interaction effects on inertia forces:

The inertia portion of the wave force on pile members is significantly different for a flexible pile structure, as compared with a corresponding rigid pile. This is because the structure accelerations are comparable in magnitude to the water particle accelerations even though the velocities differ widely.

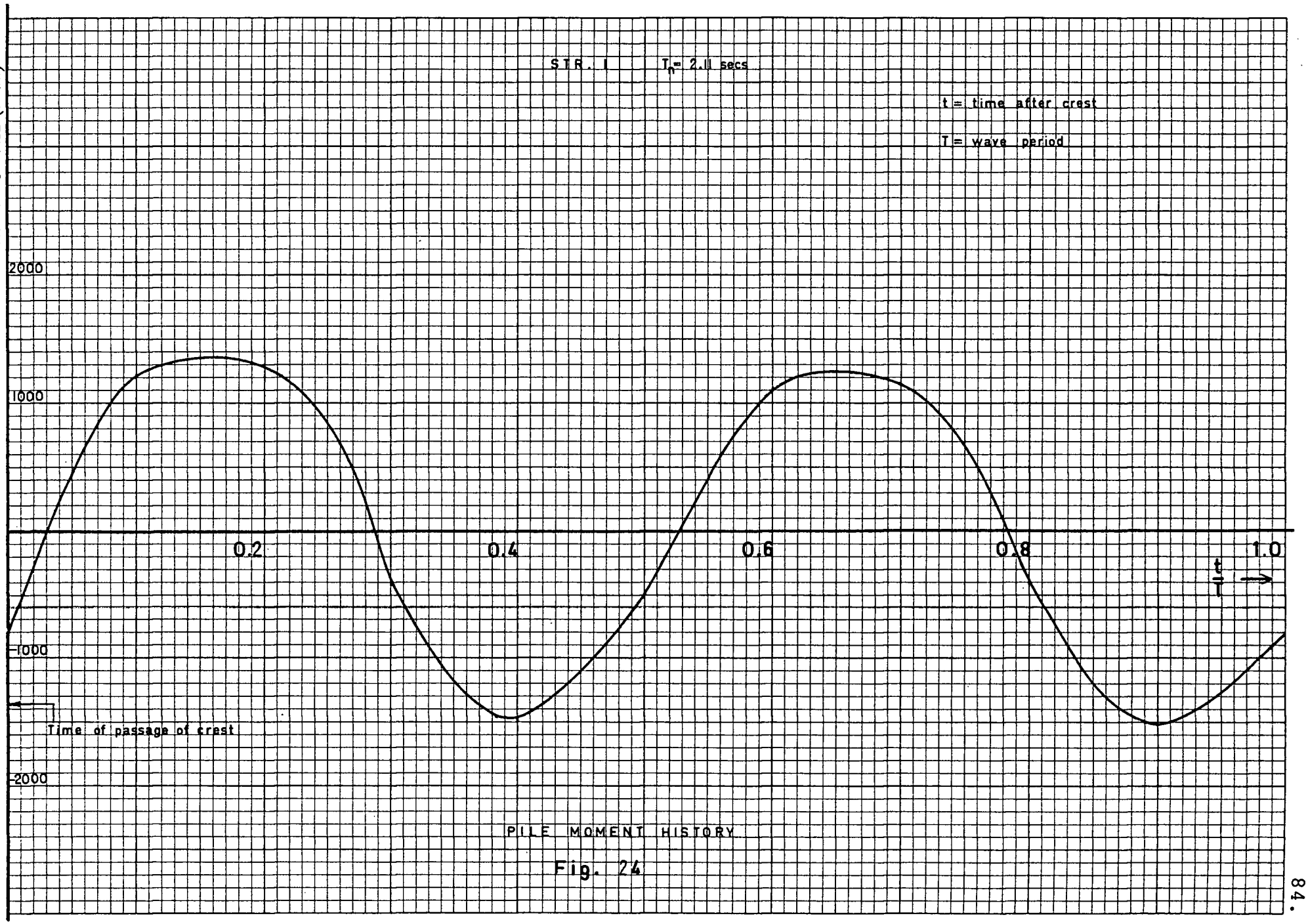


PILE MOMENT HISTORY

Fig. 24

Thus the taking into account of the feedback of structure motion in arriving at inertia force values contributes to a refinement of the response solution.

5.10 Supercritical flow conditions:

Although subcritical values of $C_D$ (1.2) were adopted for most computations in the wave problem, velocities at the surface of the water exceeded critical values for longer durations than in the earthquake situation. $N_R$ approached $2 \times 10^6$ (i.e., $> 2 \times 10^5$) based on r.m.s. velocities for the topmost node for some structures subjected to the highest waves. For 4 ft. dia. piles it approached $6 \times 10^6$ (based on r.m.s. values). This feature would reduce the wave forces. At other nodes subcritical values prevailed.

5.11 Keulegan parameter:

$\frac{V_{max.} T}{D}$ values (Ref. Section 2.18) ranged from 20 to 30, i.e., greater than 15, the value for at least one vortex to be discharged. Eddy-shedding frequencies were much lower than natural frequencies, ruling out lift resonance tendencies.

5.12 Breaking wave (solitary wave) response:

To take into account the effect of shoaling in increasing wave heights at breaking, plots of the breaker height-depth relations given by experimenters[18,19,20] were adopted.

To make use of the aforesaid relations, the point of commencement of the beach slope was taken at the point where $\frac{d}{L} = \frac{1}{2}$ (the limit for shallow water) and was used to define initial water depths. The solitary wave theory was used to find the water kinematics at the passage of the crest and thus the force levels. The parameters for the various force computations are tabulated in Table 11. The summarised particulars of the computed loads are in Table 12. The deviations of these computed forces from the true forces occur due to the following factors, whose overall effect is to warrant a slight decrease in the computed forces:

a) Increase of the statically computed member forces and stresses due to dynamic amplification.

b) Decrease: Supercritical $N_R$ values at the upper portions of the piles reduce $C_D$ in steady flow situations, this being by a factor of 3 in the upper portions.

c) Decrease: For spilling breakers and for waves deforming but not breaking under the particular slope, velocities would be lower than for a theoretical solitary wave of translation.

5.13 Comparative forces under various excitations:

Comparative values of forces and moments produced by the various wave and earthquake inputs are given in Table 13. The moments/forces for earthquake inputs have been scaled down

TABLE 11

STRUCTURAL AND OTHER PARAMETERS FOR BREAKING WAVE (SOLITARY WAVE) FORCES

| Str. No. | Height of Structure Ft. | Dia. of Main Piles D Ft. | Total Projected Area Sq. Ft. | Depth Below Trough Ft. | Height of Wave Flat Smooth Bed Ft. | Height of Wave Sloping Bed Ft. |
|---|---|---|---|---|---|---|
| I | 60 | 1.5 | 180 | 40 | - | 31 |
| II | 60 | 1.5 | 180 | 40 | - | 31 |
| IV | 90 | 3 | 405 | 60 | - | 40 |
| V | 82 | 2 | 336 | 75 | - | 45 |
| VI | 128 | 4 | 998 | 100 | - | 50 |
| VII | 128 | 2 | 468 | 100 | - | 50 |
| IX | 135 | 2 | 1013 | 95 | 50 | - |
| X | 165 | 3 | 1450 | 135 | 30 | - |

TABLE 12

LOADING DUE TO BREAKING WAVES

| Str. No. | Type of Breaker | Pile Dia. D Ft. | Total Height Of Str. Ft. | Depth of Water d Ft. | Beach Slope i | Wave $T_W$ Sec. | Characteristics $H_0$ Ft. | $H_b$ Ft. | (Proj.Area) / (Proj.Area of Pile) | Total Force on Piles K | Total Overturning Moment K.In. |
|---|---|---|---|---|---|---|---|---|---|---|---|
| I,II,III | Spilling | 1.5 | 60 | 40 | .05 | 10 | 33 | 31 | 1.11 | 128 | 63600 |
| IV | Plunging (.05) Spilling (.02,.01) | 3 | 90 | 60 | .05,.02,.01 | 10 | 40 | 40 | 1.0 | 230 | 171100 |
| V | Plunging (.05) Spilling (.02,.01) | 2 | 82 | 75 | .05,.02,.01 | 12 | 50 | 45 | 1.06 | 266 | 214800 |
| VI | Spilling | 4 | 128 | 100 | .02,.01 | 10 | 55 | 50 | 1.02 | 735 | 783000 |
| VII | Spilling | 2 | 128 | 100 | .02,.01 | 10 | 55 | 50 | 1.05 | 367 | 391000 |
| IX | Spilling | 2 | 135 | 120 | 0 | 10 | 50 | 50 | 1.13 | 950 | 960000 |
| X | Unspecified | 3 | 165 | 150 | 0 | 16 | 50 | - | 1.13 | a) *303 | 270000 |
| | | | | | | | | | | b) †950 | 960000 |

N.B. *Lower limit (under linear oscillatory waves) † Upper limit: as for IX

1. Static calculations for moments.
2. Beach slopes are indicated in parentheses.
3. $C_D = 1.2$

TABLE 13

COMPARATIVE VALUES OF MOMENTS AND AXIAL FORCES UNDER VARIOUS EXCITATIONS

| Str. No. | $T_n$ Secs. | $\omega_n$ | d Ft. | Oscillatory Linear Waves: Worst Mom. K" | Oscillatory Linear Waves: Worst Axial Force K | Stokes Shallow Water Waves: Worst Mom. K" | Stokes Shallow Water Waves: Worst Axial Force K | Breaking Waves: Beach Slope | Breaking Waves (Scaled by 0.75): Worst Mom. K" | Breaking Waves (Scaled by 0.75): Worst Axial Force K | El Centro Quake Response Spectrum (Scaled for Yielding): Worst Mom. K" | El Centro Quake Response Spectrum (Scaled for Yielding): Worst Axial Force K |
|---|---|---|---|---|---|---|---|---|---|---|---|---|
| I | 2.11 | 2.98 | 40 | 302*1 | 1 | 950<br>940 | 240<br>270 | 0.05 | 2770 | 13 | 1185 | 143 |
| II | 2.65 | 2.37 | 40 | - | - | 3200<br>3160 | 230<br>640 | 0.05 | 4500 | 10 | 1850<br>1550 | 140<br>40 |
| III | 3.45 | 1.82 | 40 | - | - | 2180 | 240 | 0.05 | 2340 | 25 | 890*2 | 85 |
| V | 1.44 | 4.36 | 75 | - | - | 396<br>156 | 55<br>1309 | 0.05<br>0.02,0.01 | 2410<br>2910 | 18<br>95 | 787<br>415 | 92<br>330 |
| VI | 2.55 | 2.46 | 100 | 13000 | 250 | 23100<br>3500 | 1480<br>2170 | 0.02,0.01 | 11500<br>2450 | 290<br>5020 | 5400<br>1030 | 215<br>2050 |
| VII | 2.84 | 2.21 | 100 | 3500*3 | 10 | 5550<br>1540 | 0<br>1030 | 0.02,0.01 | 1210<br>2300 | 720<br>17 | 800<br>250 | 100<br>450 |
| VIII | 0.99 | 6.29 | 200 | 1231 | 304 | 1250 | 300 | 0 | 4830 | 1360 | 2720@ | 760@ |
| IX | 1.18 | 5.33 | 120 | - | - | - | - | 0 | 3400 | 1480 | 1090 | 625 |
| X | 0.80 | 7.97 | 150 | 1680 | 500 | - | - | 0 | 3400 | 1480*4 | 2110 | 670 |
| XI | 0.99 | 6.29 | 250 | 1900 | 510 | - | - | 0 | 3350 | 610 | 3200 | 735 |
| XII | 4.48 | 1.40 | 800 | 31800000† | - | - | - | - | - | - | 280000 | - |
| XIII | 6.28 | 1.00 | 1200 | % | - | - | - | - | - | - | + | - |

*1 Static application of shallow water wave forces.
*2 Estimated.
*3 Concentration of load at a point assumed.
*4 Estimated.
@ Exact elastic values by time step integration: Mom.: 6500 K"; Axial force: 1800K.
† 3 standard deviations. Ref.: Foster, E.T.: Model for nonlinear dynamics of offshore towers (J.A.S.C.E. Vol. 96, No.EM1, Feb.1970).
% 3 standard deviations of displacement at top = 2.7 ft. Ref.: Malhotra A, and Penzien J.: Response of offshore structures to random wave forces (J.A.S.C.E. Vol. 96, No. ST.10, October, 1970).
+ Displacement at top in elastic behaviour = 1.33 ft.

by a half to allow for the reduction in design forces that would result from ductile yielding of the structural members. This is conservative when compared to current earthquake design philosophy of structures.[16] For reasons quoted in Section 5.12, the computed breaking wave moments/forces have been scaled down by 25 percent. The comparative values of stresses are given in Table 14.

Some of the parameters that have a bearing on comparative responses are:

1) natural period
2) water depth
3) diameter of piles
4) mass/(member stiffness) ratio
5) bed slope.

Other parameters such as i) depth of water at the toe of the beach slope, ii) bed roughness, etc. would also be relevant, especially for breaking wave forces.

For each structure the critical load case, as well as depth d and period $T_n$, have been noted in Table 15. From considerations discussed in previous sections and chapters, the natural period $T_n$ and the water depth d were adjudged to be the parameters most materially affecting the comparative response.

TABLE 14

COMPARATIVE STRESSES

| Str. No. | $T_n$ | X-section Area | X-section $I$ In.$^4$ | X-section $d$ Ft. | Stresses (K/in.$^2$) Osc. Linear Waves | Stokes' Shallow Water Waves | Breaking Waves | El Centro Quake Response Spectrum Masses at Top (K) | El Centro Quake Response Spectrum Stresses |
|---|---|---|---|---|---|---|---|---|---|
| I | 2.11 | 31 | 861 | 40 | ±3.1+0.03 | ±9.9+ 7.7<br>±9.8+ 8.7 | ±38.7+ 0.5 | 2x150 | ±9.4+ 3.9 |
| II | 2.65 | 31 | 861 | 40 | - | ±33.5+ 7.4<br>±32.9+20.6 | ±47.1+ 0.3 | 2x150 | ±19.4+ 1.3 |
| III | 3.45 | 7.1 | 287 | 40 | | Unrepresentative Structure | | | |
| IV | 4.4 | 56 | 800 | 60 | | " | " | | |
| V | 1.44 | 28 | 1200 | 75 | - | ±4.0+ 2.0<br>±1.6+46.8 | ±38.8+ 4.5 | 2x200 | ±7.9+ 3.3<br>±4.2+11.7 |
| VI | 2.55 | 112 | 21000 | 100 | ±14.8+2.2 | ±26.4+13.2<br>± 4.0+19.4 | ±17.5+ 3.4<br>±3.7+59.8 | 2x500 | ±6.2+ 1.9<br>±1.2+18.3 |
| VII | 2.84 | 28 | 1360 | 100 | ±31.0+0.4 | ±49.1+ 0<br>±13.6+36.8 | ±14.4+34.1<br>±27.1+ 0.8 | 2x300 | ±7.1+ 3.6<br>±2.2+16.1 |
| VIII | 0.99 | 85 | 12600 | 200 | ±1.8+3.6 | ±1.8+ 3.6 | ±6.9+16.0 | 2x400 | ±3.9+ 8.9* |
| IX | 1.18 | 37.7 | 2720 | 120 | - | - | ±15.0+39.2 | 2x400 | ±4.0+13.8 |
| X | 0.80 | 56.5 | 9170 | 150 | ±3.3+8.9 | - | ±6.7+26.2 | 2x400 | ±3.5+ 9.9 |
| XI | 0.99 | 126 | 18900 | 250 | ± 2.4+4.0 | - | ± 4.3+ 4.8 | 2x320 | ± 4.1+ 5.8 |

*Exact values (by time step integration) for elastic behaviour: ±5.2+11.9 K/in.$^2$

TABLE 15

GOVERNING LOAD CASES FOR OFFSHORE TOWERS

| Structure | $T_n$ Secs. | d Ft. | Governing Load |
|---|---|---|---|
| I | 2.11 | 40 | Breaking (Solitary) wave |
| II | 2.65 | 40 | Breaking (Solitary) wave |
| III | 3.45 | 40 | Breaking (Solitary) wave |
| V | 1.44 | 75 | Breaking (Solitary) wave |
| VI | 2.55 | 100 | Shallow water oscillatory wave |
| VII | 2.84 | 100 | Shallow water oscillatory wave |
| VIII | 0.99 | 200 | 1. Breaking wave 2. Earthquake |
| IX | 1.18 | 120 | Breaking wave |
| X | 0.80 | 150 | 1. Breaking wave 2. Earthquake |
| XI | 0.99 | 250 | Earthquake |

LOAD TYPES

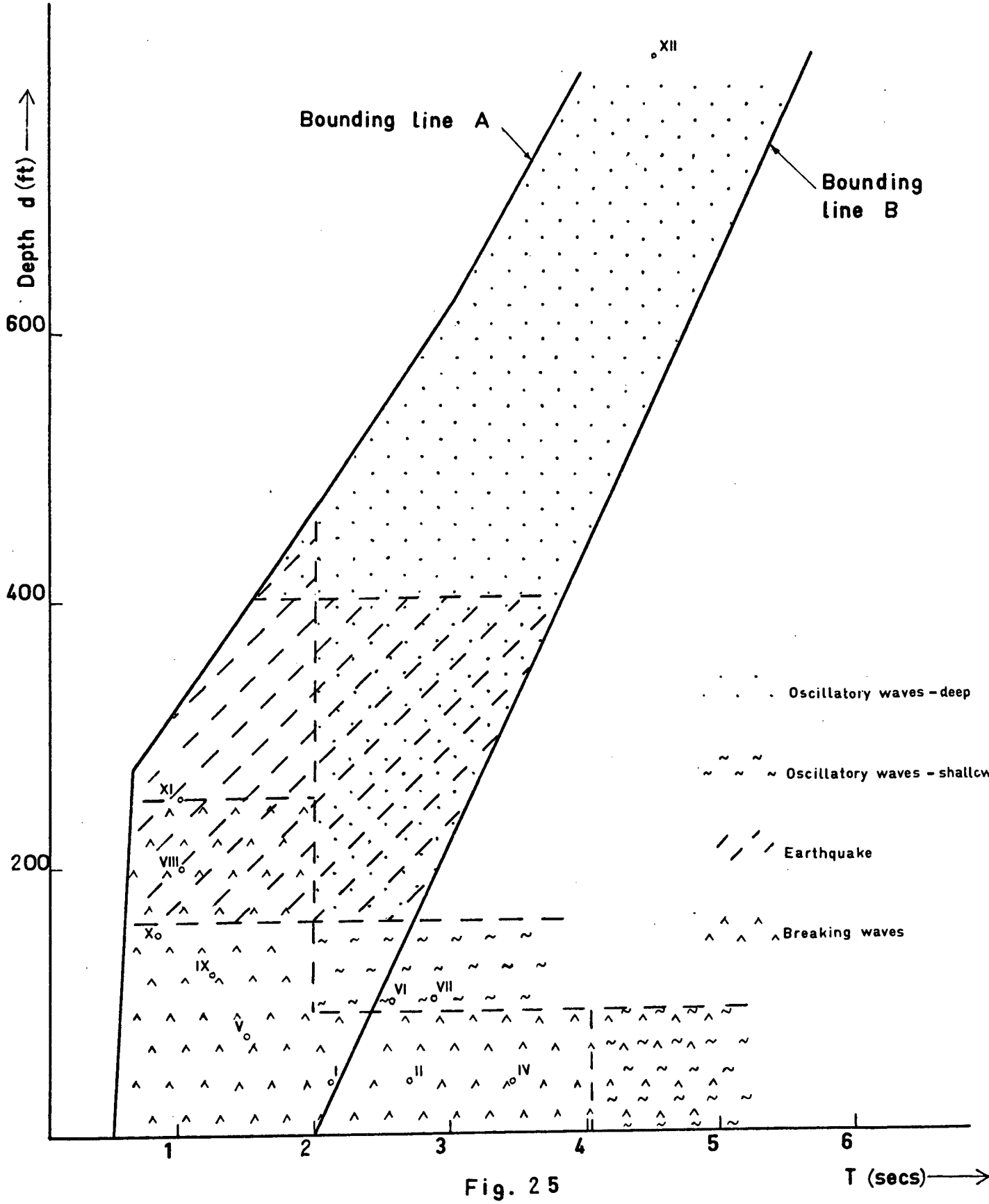


Fig. 25

The fundamental period $T_n$ is the most important system characteristic that principally determines the degree of resonance with excitations with various dominant frequencies. Since the offshore structures were taken as geometrically almost similar, and the increase in masses was graded in relation to depth, it also follows that for a given d, the period $T_n$ indirectly reflects member cross-sectional sizes.

In the case of oscillatory waves, the water depth influences the maximum wave dimensions, the contact area, and the relative magnitudes of higher harmonics of nonlinear waves; in the case of breaking waves it determines the height and velocity distribution of the wave and the contact area. For these reasons a plot in the d-$T_n$ space corresponding to the type of loading that may govern design has been made and is shown in Fig. 25. In constructing this plot attention was restricted to the region between the two bounding lines A and B since practical structures would not likely fall outside this region. Depending on the values of d and $T_n$, four different load types were found to govern, these being i) oscillatory waves in shallow water, ii) breaking waves, iii) earthquakes and iv) oscillatory waves in deep water. Between the zones where an individual load case governs, transition zones are shown where two adjacent types are equally likely to govern.

5.14 Broad ranges of influence of load types:

In overview the plot in Fig. 25 is seen to highlight the following:

i) the dominant influence of breaking wave forces on structures with depths less than 90 ft. and to a certain extent on those with depths less than 160 ft.

ii) the dominant influence of earthquake loads on structures with natural periods less than 2 sec.

iii) the importance of designing on the basis of periodic deep water waves for structures with a d-T combination falling outside i) or ii).

# CHAPTER VI

# CONCLUSIONS

## 6.1 Effects of mass coefficient:

Virtual mass effects have to be examined in detail in determining response to earthquake motion for bulky submerged structures with large periods. In the case of such structures this would necessitate determining the virtual mass coefficients corresponding to the variable flow phases. A conclusive relationship of $C_M$ to the flow parameters was not established, although a possible one, based on limited experimental data, has been suggested. It was observed that for some of the structures considered, the peak earthquake-induced displacements increased by about 25 percent for the highest values of $C_M$ over those for zero added $C_M$.

## 6.2 Shallow water waves:

As regards water wave inputs in shallow water, large dynamic displacements would be sustained only by flexible structures with periods well over 2 seconds. The greatest wave forces occur at or near the time of the passage of the crest.

## 6.3 Load types governing design:

A graphical relationship is presented showing the load type, such as earthquake or wave forces, that governs the design of offshore structures. The two parameters that govern the load

type are the natural period of the structure and the water depth. The choice of these as the basic independent parameters and as being the principal determinants of the comparative response under various types of excitation, was based on the following considerations:

a) the fundamental period $T_n$ is the characteristic that mainly influences dynamic response to inputs of differing frequencies.

b) the water depth d determines the maximum wave dimensions and the water contact area. In the case of oscillatory waves, it also influences the relative magnitudes of higher harmonics of nonlinear waves that induce structural resonance and moreover, in the case of breaking waves it determines the velocity distribution in the wave. The water depth also influences the overall structural size and hence the natural frequency.

c) other material parameters are reflected in some form in these two parameters.

The resulting plot of the d-T space in Fig. 25 delineates the regions where various types of ocean waves and earthquake loading would govern design. The various regions are located within a pair of bounding lines which constitute a restriction on practical structural geometries.

From an overall point of view the following broad trends appear in the various areas of the plot:

i) the dominant influence of breaking wave forces in the design of structures with water depths less than 90 feet, and also to a lesser extent, on those with depths less than 160 feet.

ii) the appropriateness of considering earthquake loads in the design of structures with periods less than 2 seconds

iii) the dominant influence of periodic deep water waves on offshore structures in the rest of the d-T region.

The effects of other kinds of loading such as dead loads and water currents can be superposed without affecting the relative preponderance of the effect of one of the above load types.

This plot is a useful aid in preparing a first design of a shallow or deep water structure of the platform deck type.

6.4 Other conclusions:

a) In the shallow water range, manipulation of pile spacing would not significantly reduce wave response, but structural geometry and the design of structural modal frequencies widely separated from the frequencies of the higher waves would do so.

b) The steady-state response to waves as computed is considerably less when the interaction between water and structure velocities is considered than when it is ignored.

c) Wave forces in the large wave-height range are predominantly drag forces whereas fluid forces under an earthquake excitation are mainly inertia forces.

d) The ranges of water velocity and pile diameter where the magnitude and frequency of lift are important have been specified. Combined response in longitudinal and lateral directions taking into consideration lift forces should be studied for structures with periods greater than 3 seconds. For the structures considered here the lift forces were negligible.

# BIBLIOGRAPHY


1. Wiegel, R.L. Oceanographical engineering: Prentice-Hall, Inc., Englewood Cliffs, N.J.: 1964.

2. Kinsman, B. Wind waves: Prentice Hall, Inc., Englewood Cliffs, N.J.: 1965.

3. Ippen, A.T. Estuary and coastline hydrodynamics: Engineering Societies Monographs: McGraw-Hill Book Co., Inc.: 1966.

4. Morison, J.R. et al. The force exerted by surface waves on piles: Petroleum Transactions, A.I.M.M.E. Vol. 189, 1950.

5. Hino, M. A theory on the fetch graph, the roughness of the sea and, the energy transfer between wind and wave: Proc. 10th Conference on Coastal Engineering, 1966.

6. Bretschneider, C.L. and Reid, R.O. Surface waves and offshore structure, etc.: Technical report, October, 1953, The Texas A. & M. Research Foundation.

7. Camfield, F.E. and Street R.L. Observations and experiments on solitary wave deformation: 10th Conference on Coastal Engineering, Vol. I, 1966.

8. Hall, M.A. Laboratory study of breaking wave forces on piles: Beach Erosion Board T. Memo. No. 106, August, 1958.

9. Laird, A. Water forces on flexible oscillating cylinders: Journal Waterways and Harbors Division, A.S.C.E., Vol. 88, No. WW3, August 1962.

10. Keulegan, G.H. and Carpenter, L.H. Forces on cylinders and plates in an oscillatory fluid: Journal National Bureau of Standards, Vol. 60, No. 5, May 1958.

11. Sarpkaya, T. and Garrison C.J. Vortex formation and resistance in unsteady flow: Journal Applied Mechanics, Trans. A.S.M.E., Vol. 85, Series E, March, 1963.

12. Agerschou, H.A. and Edens, J.J. 5th and 1st order wave force coefficients for cylindrical piles: Coastal Engineering, Santa Barbara Specialty Conference, October, 1965.

13. McNown, J.S. Drag in unsteady flow: IX Congres International de Mecanique Appliquee, Actes, Tome III, 1957.

14. McNown, J.S. and Keulegan, G.H. Vortex formation and resistance in periodic motion: Journal Engineering Mech. Div., A.S.C.E., Vol. 85, EM 1, Part 1, January, 1959.

15. Paape, A. and Breusers, H. The influence of pile dimension on forces exerted by waves: Proc. 10th Conference on Coastal Engineering, Vol. II, A.S.C.E., 1967.

16. Blume, J.A., Corning, L.H. and Newmark, N.M. Design of multistory reinforced concrete buildings for earthquake motions: Pub.'s Portland Cement Association.

17. Mason, M.A. Tax transformation of waves in shallow water: Proceedings of 1st Conference on Coastal Engineering, Council on Wave Research, 1950.

18. Iversen, H.W. Waves and breakers in shoaling water: Proceedings of 3rd Conference on Coastal Engineering, 1952.

19. Nakamura, M., Shiraishi, H. and Sasaki, Y. Wave decaying due to breaking: Proceedings of 10th Conference on Coastal Engineering, A.S.C.E., 1966.

20. Kishi, T. and Saeki, H. The shoaling, breaking and run-up of the solitary wave on impermeable rough slopes: Proc. 10th Conference on Coastal Engineering, A.S.C.E., 1966.

21. Laird, A.D.K., Johnson, C.A. and Walker, R.W. Water forces on accelerated cylinders: Journal Waterways and Harbors Division, A.S.C.E., Proc. Vol. 85, No. W.W.1, 1959.

22. Laird, A.D.K., Johnson, C.A. and Walker, R.W. Water eddy forces on oscillating cylinders: Journal of the Hydraulics Division, A.S.C.E., Vol. 86, No. HY9, November, 1960.

23. Laird, A.D.K. Eddy forces on rigid cylinders: Journal of Waterways and Harbors Division, A.S.C.E., Vol. 87, No. W.W.4, November, 1961.

24. Laird, A.D.K. and Warren R.P. Groups of vertical cylinders oscillating in water: Journal of Engineering Mechanics Division, A.S.C.E., Vol. 89, No. EM 1, February, 1963.

25. Laird, A.D.K. Forces on a flexible pile: A.S.C.E. Specialty Conference on Coastal Engineering, Santa Barbara, California, October, 1965.

26. Wiegel, R.L. Earthquake engineering: Prentice Hall, 1970.

# APPENDIX I

## CAUSES OF DISPARITIES BETWEEN WAVE FORCE COEFFICIENT DATA

1) Most experimenters used values for water velocities which were computed instead of being measured during the wave force experiments. The true velocities, it is concluded, differed from the computed values to varying extents. Another source of divergence was that some experimenters measured the velocities at the crest or at some other point and related the drag coefficients to the measured ones.

2) Some experimenters used the linear theory in computing velocity values whereas others used nonlinear theories.

3) Neglect of the random variation of the wave form in prototype tests.

4) The effect of parameters, which could not be pinpointed, other than $N_R$.

5) Uncertain knowledge of the diffusion of turbulence.

6) Neglect of the convectional terms of the acceleration $\frac{Du}{Dt}$ in the force expressions.

7) Varying roughness and flexibility of the models and prototypes.

8) Vibrations of test piles.

9) Turbulence around the structures by which the prototype test piles were supported.

# APPENDIX II

## WAVE THEORIES

The time period of ocean waves and their heights have been correlated experimentally with wind inputs (fetches, wind speeds and duration). For computations of the characteristics of deterministic wave forces, the period and height would be known independent data.

### Linear Theory

For a simple harmonic wave progressing in the x-direction with phase velocity $C_{ph}$ as shown in Fig. 26, the differential equation to be satisfied[2] for all x and within $-d \leq z \leq \eta$ is

$$\frac{\partial^2 \phi}{\partial x^2} + \frac{\partial^2 \phi}{\partial x^2} = 0 \qquad \text{(II-1)}$$

where $\phi$ is the velocity potential function such that

$$\text{Horizontal velocity } u = -\frac{\partial \phi}{\partial x}; \quad \text{Vertical velocity } w = -\frac{\partial \phi}{\partial z} \qquad \text{(II-2)}$$

The boundary condition at the bottom is:

$$\begin{aligned} W &= -\frac{\partial \phi}{\partial z} = 0 \qquad \text{on } z = -d \\ u &= -\frac{\partial \phi}{\partial x} = 0 \qquad \text{on } z = -d \end{aligned} \qquad \text{(II-3)}$$

The condition on the upper boundary is a mixed boundary condition:

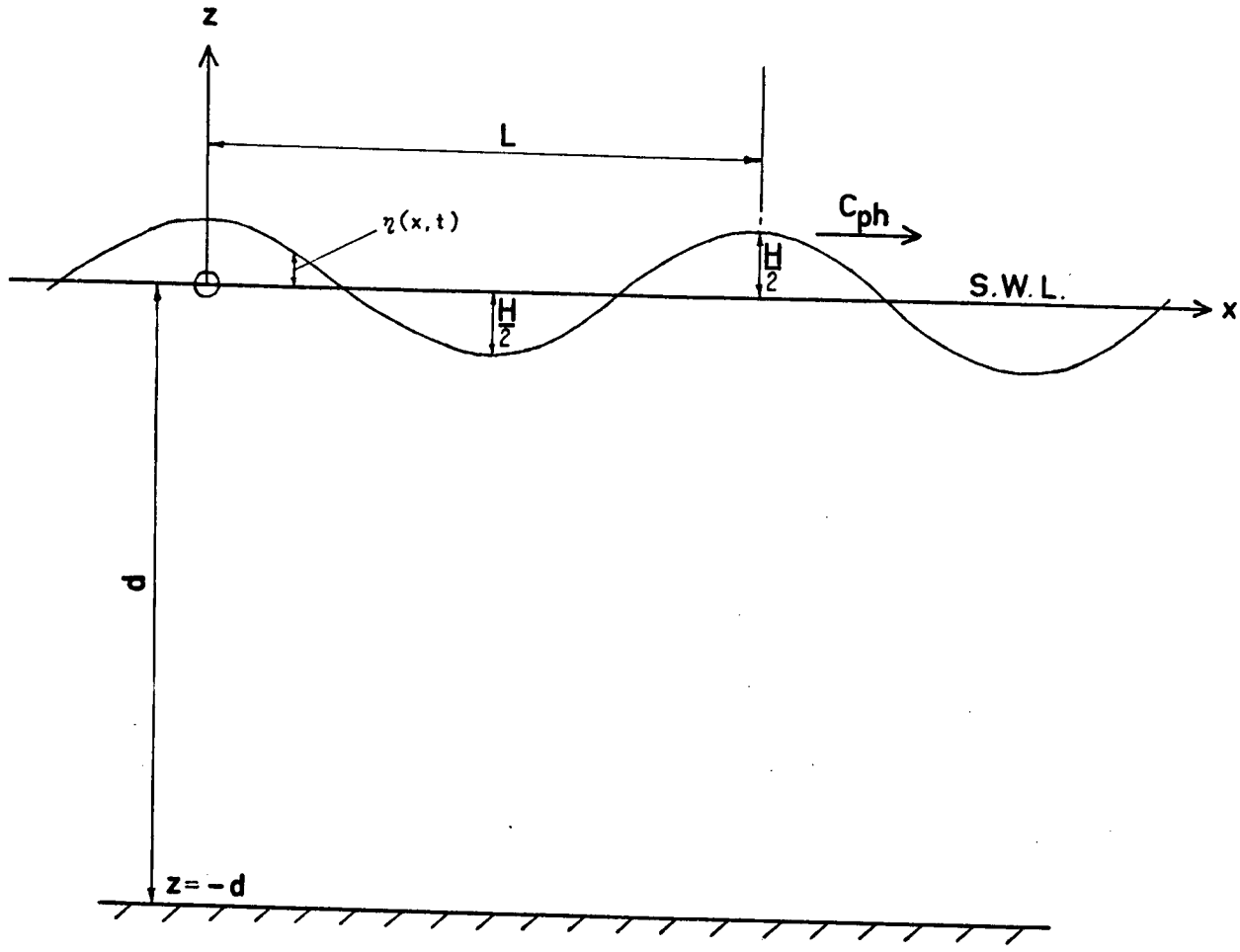


LINEAR WAVE

Fig 26

$$-\frac{\partial\phi}{\partial t}\Big|_{z=\eta} + \frac{1}{2}(u^2 + w^2) + \frac{p}{\rho}\Big|_{z=\eta} + gz\Big|_{z=\eta} = 0$$

where $p$ = fluid pressure (zero at free surface)

$\rho$ = mass density of the fluid

Since

$$u^2 << \frac{\partial\phi}{\partial t} \quad ; \quad w^2 << \frac{\partial\phi}{\partial t}$$

this becomes $$\eta = \frac{1}{g}\frac{\partial\phi}{\partial t} \qquad \text{on } z = \eta$$

In the small-amplitude linear theory this is simplified to

$$\eta = \frac{1}{g}\frac{\partial\phi}{\partial t} \qquad \text{on } z = 0 \qquad \text{(II-4)}$$

The general solution of equation (II-1) is of the form

$$\phi = C_1+C_2x+C_sz+(C_4\cos C_8x+C_5\sin C_8x)(C_6e^{C_8z}+C_7e^{-C_8z})$$

or equivalently

$$\phi = C_1+C_2x+C_3z+(C_4\cos C_8x+C_5\sin C_8x)\{C_9\cosh C_8(z+C_{11})$$

$$+C_{10}\sinh C_8(z+C_{12})\}$$

Using the spatial periodicity of $\phi$ at intervals of length L,

$$C_2 = 0$$

$$C_8 = \frac{2\pi}{L}$$

Having chosen the moving origin of coordinates at the crest means

$$C_5 = 0$$

$$C_4 \neq 0$$

The zero net transport of fluid in the vertical direction yields

$$C_3 = 0.$$

Use of the condition II-3 makes

$$C_{10} = 0$$

$$C_{12} = d$$

$$\phi = C_4 C_9 \cosh\{\frac{2\pi}{L}(z+d)\} \sin\frac{2\pi}{L} x$$

Changing the moving origin of coordinates to a fixed one, velocity being $\frac{L}{T}$

$$\phi = C_4 C_9 \cosh\{\frac{2\pi}{L}(z+d)\}\sin(\frac{2\pi}{L} x - \frac{2\pi}{T}t)$$

Use of II-4 and a velocity $u = \frac{L}{T}$ at $z = \frac{H}{2}$ yields

$$\phi = C_{ph} \frac{H}{2} \frac{\cosh 2\pi(z+d)/L}{\sinh 2\pi d/L} \sin(\frac{2\pi}{L} x - \frac{2\pi}{T}t) \qquad \text{(II-5)}$$

where $C_{ph} = \frac{L}{T}$.

The velocities are then derived:

Horizontal Velocity component

$$u = \frac{\pi H}{T} \frac{\cosh \frac{2\pi(z+d)}{L}}{\sinh 2\pi d/L} \cos\left(\frac{2\pi}{L} x - \frac{2\pi}{T} t\right) \qquad \text{(II-6)}$$

Vertical component $w = \frac{\pi H}{T} \frac{\sinh \frac{2\pi(z+d)}{L}}{\sinh 2\pi d/L} \sin\left(\frac{2\pi}{L} x - \frac{2\pi}{T} t\right)$ (II-7)

Surface elevation $\eta = \frac{H}{2} \cos\left(\frac{2\pi}{L} x - \frac{2\pi}{T} t\right)$ (II-8)

Specialising to the case of deep water $\left(\frac{d}{L} > \frac{1}{2}\right)$,

Length of wave $L_0 \doteq \frac{gT^2}{2\pi}$ (II-9)

Wave phase velocity $C_{ph} = \frac{L}{T}$

$$\doteq \frac{gT}{2\pi} \qquad \text{(II-10)}$$

Variations of pressure with depth are negligible.

Finite-Amplitude Stokes Theory

This theory[2,3] starts with the assumptions that the motion is irrotational and both potential $\phi$ and stream function $\psi$ exist. The free surface boundary condition is however different from the linear case.

The solution of

$$\nabla^2 \psi = 0 \qquad \text{(II-11)}$$

subject to the boundary conditions as under, with a moving system of coordinate axes,

$$\psi\Big|_{z=\eta} = 0$$

$$\psi\Big|_{z=-d} = k_1$$

$$g\eta + \frac{1}{2}\left[\left(\frac{\partial\psi}{\partial z}\right)^2 + \left(\frac{\partial\psi}{\partial x}\right)^2\right]\Bigg|_{z=\eta} = k_3$$

is found to be

$$\psi(x,z) = C_1 z + C_2 + (C_3 \cos C_7 x + C_4 \sin C_7 x)\,(C_5 e^{C_7 z} + C_6 e^{-C_7 z}) \qquad \text{(II-12)}$$

Using the conditions of

1) spatial periodicity at intervals of length L
2) vertical velocity at bottom for $d\to\infty$ being zero
3) horizontal velocity at bottom for $d\to\infty$ being zero

$$C_6 = 0$$

$$C_1 = C_{ph}$$

where $C_{ph}$ = speed of motion of the coordinate axes.

$$\psi(x,z) = -C_{ph} z + C_2 + C_5 e^{\kappa z}\,(C_3 \cos\kappa x + C_4 \sin\kappa x)$$

where $\kappa = \frac{2\pi}{L}$

Since $\psi\Big|_{z=\eta} = 0$ for all $\eta$,

$$C_2 = 0$$

$\frac{\psi(x,z)}{C_{ph}} = -z + \beta e^{\kappa z}\cos\kappa x$ is a particular solution if

$$\beta = \frac{C_3 C_5}{C_{ph}} \qquad \text{(II-13)}$$

and $$C_4 = 0$$

Using Cauchy-Riemann relations, the potential function $\phi$ is found

$$\frac{\phi(x,z)}{C_{ph}} = -x + \beta e^{\kappa z}\sin\kappa x.$$

From the expression for $\psi$, putting $z = \eta$,

$$\eta = \beta e^{\kappa\eta}\cos\kappa x$$

$$\eta = \beta[1+\kappa\eta+\frac{1}{2}(\kappa\eta)^2+\frac{1}{6}(\kappa\eta)^3+\ldots]\cos\kappa x \qquad \text{(II-14)}$$

Stokes' Third Order Theory[2,3]

Approximate values for $\eta, \psi$ and $\phi$ are given by this theory correct to the third order in $\beta$.

Expressing $\eta$ as

$$\eta = \beta\eta_0 + \beta^2\eta_1 + \beta^3\eta_2$$

and substituting

$$\beta\eta_0 + \beta^2\eta_1 + \beta^3\eta_2 = F(\beta,\eta_0,\eta_1,\eta_2,\kappa,x)$$

Retaining terms only up to $\beta^2$,

$$\eta_0 + \beta\eta_1 + \beta^2\eta_2 = [\cos\kappa x]+\beta[\kappa\eta_0\cos\kappa x]+\beta^2[(\kappa\eta_1+\tfrac{1}{2}\kappa^2\eta_0{}^2)\cos\kappa x]$$

equating coefficients of $\beta^0$, $\beta^1$ and $\beta^2$ respectively,

$$\eta_0 = \cos\kappa x$$

$$\eta_1 = \kappa\eta_0 \cos\kappa x = \tfrac{1}{2}\kappa + \tfrac{1}{2}\kappa \cos 2\kappa x$$

$$\eta_2 = (\kappa\eta_1+\tfrac{1}{2}\kappa\eta_0^2)\cos\kappa x = \tfrac{9}{8}\kappa^2\cos\kappa x + \tfrac{3}{8}\kappa^2 \cos 3\kappa x.$$

Therefore $\eta = \frac{1}{2}\kappa\beta^2 + \beta(1+\frac{9}{8}\kappa^2\beta^2)\cos\kappa x + \frac{1}{2}\kappa\beta^2 \cos 2\kappa x+\frac{3}{8}\kappa^2\beta^3\cos 3\kappa x$

(II-15)

The coefficient of cos $\kappa x$ is rearranged, letting $a = \beta(1+\frac{9}{8}\kappa^2\beta^2)$

Solving for $\beta$, $\beta = \varepsilon_1 a + \varepsilon_2 a^2 + \varepsilon_3 a^3 + \ldots$

or $a = \varepsilon_1 a + \varepsilon_2 a^2 + \varepsilon_3 a^3 + \frac{9}{8}\kappa 2(\varepsilon_1 a+\varepsilon_2 a^2+\varepsilon_3 a^3)^3$

Retaining terms upto 3rd power of a and equating coefficients of like powers, $\beta$, $\varepsilon_1$, $\varepsilon_2$ and $\varepsilon_3$ are obtained, and then

$$\eta = \tfrac{1}{2}\kappa a^2 + a \cos\kappa x + \tfrac{1}{2}\kappa a^2\cos 2\kappa x + \tfrac{3}{8}\kappa^2 a^3\cos 3\kappa x \quad \text{(II-16)}$$

Choosing a new moving origin of coordinates at $z = \frac{1}{2}\kappa a^2$

$$\eta = a \cos\kappa x + \tfrac{1}{2}\kappa a^2 \cos 2\kappa x + \tfrac{3}{8}\kappa^2 a^3 \cos 3\kappa x \quad \text{(II-17)}$$

Substitution of $\beta = \varepsilon_1 a + \varepsilon_2 a^2 + \varepsilon_3 a^3$

$$\doteq a - \tfrac{9}{8}\kappa^2 a^3$$

in the expressions for $\phi$, yield $\phi$, and by differentiation, the components of velocity. The expression changes for fixed coordinates to

$$\eta = a\cos(\kappa x-\frac{2\pi}{T}t)+\frac{1}{2}\kappa a^2\cos 2(\kappa x-\frac{2\pi}{T}t)+\frac{3}{8}\kappa^2 a^3\cos 3(\kappa x-\frac{2\pi}{T}t) \qquad \text{(II-18)}$$

Stokes' Third Order Theory--Finite Depth

Similar to the foregoing derivation for the case when $d\to\infty$, a perturbation technique applied to the solutions $\phi$, $\psi$, $\eta$ and celerity $C_{ph}$ and application of the surface and bottom boundary conditions yield[1,3] the general third order relations:

Wave profile

$$\eta = a\cos(\kappa x-\frac{2\pi}{T}t)+\frac{\pi a^2}{L}f_2\cos 2(\kappa x-\frac{2\pi}{T}t)+\frac{\pi^2 a^3}{L^2}f_3\cos 3(\kappa x-\frac{2\pi}{T}t) \qquad \text{(II-19)}$$

where $f_2 \equiv f_2(\frac{d}{L}) = \dfrac{(2+\cosh 4\pi d/L)\cosh 2\pi d/L}{2\sinh^3\frac{2\pi d}{L}}$

$$f_3 \equiv f_3(\frac{d}{L}) = \frac{3}{16}\frac{1+8\cosh^6 2\pi d/L}{\sinh^6 2\pi d/L}$$

Wave height $H = 2a + \dfrac{2\pi^2}{L^2}a^3 f_3(\frac{d}{L})$ (II-20)

Horizontal velocity $u = C_{ph}[F_1\cosh\frac{2\pi(z+d)}{L}\cos(\kappa x-\frac{2\pi}{T}t)+F_2\cosh\frac{4\pi(z+d)}{L}$

$$\cos 2(\kappa x-\frac{2\pi}{T}t)+F_3\cosh\frac{6\pi(z+d)}{L}\cos 3(\kappa x-\frac{2\pi}{T}t)] \qquad \text{(II-21)}$$

and horizontal local acceleration $\frac{\partial u}{\partial t}$

$$\frac{\partial u}{\partial t} = \frac{2\pi C_{ph}}{T} F_1 \cosh\frac{2\pi(z+d)}{L} \sin(\kappa x - \frac{2\pi}{T}t) + \frac{4\pi C_{ph}}{T} F_2 \cosh\frac{4\pi(z+d)}{L}$$

$$\sin 2(\kappa x - \frac{2\pi}{T}t) + \frac{6\pi C_{ph}}{T} F_3 \cosh\frac{6\pi(z+d)}{L} \sin 3(\kappa x - \frac{2\pi}{T}t) \quad \text{(II-22)}$$

where $F_1 = \frac{2\pi a}{L} \frac{1}{\sinh\frac{2\pi d}{L}}$

$$F_2 = \frac{3}{4} (\frac{2\pi a}{L})^2 \frac{1}{\sinh^4\frac{2\pi d}{L}}$$

$$F_3 = \frac{3}{64} (\frac{2\pi a}{L})^3 [\frac{11-2\cosh\frac{4\pi d}{L}}{\sinh^7\frac{2\pi d}{L}}]$$

$$C_{ph} = \sqrt{\frac{gL}{2\pi}\tanh\frac{2\pi d}{L}[1+(\frac{\pi a}{L})^2 \frac{14+4\cosh^2\frac{4\pi d}{L}}{16\sinh^4\frac{2\pi d}{L}}]} \quad \text{(II-23)}$$

$$L = \frac{gT^2}{2\pi}\tanh\frac{2\pi d}{L} [1+(\frac{2\pi a}{L})^2 (\frac{14+4\cosh^2\frac{4\pi d}{L}}{16\sinh^4\frac{2\pi d}{L}})] \quad \text{(II-24)}$$

The above development presupposes that the wave length L is known. L is to be found from the nonlinear relation at (II-24) above.

Solitary Wave Theory

This represents a wave with the entire water body lying above the original water level, and mathematically the water particles move only in the direction of wave advance. As Fig. 16 shows the wave length is infinite. The equations for the

water profile and wave velocity are:

$$y_s = d+H \operatorname{sech}^2[\sqrt{\frac{3}{4}\frac{H}{d^3}}(x-Ct)] \qquad \text{(II-25)}$$

$$C = \sqrt{gd}\,(1+\frac{1}{2}\frac{H}{d})$$

$$\doteq \sqrt{gd(1+\frac{H}{d})} \qquad \text{(II-26)}$$

These are correct to the 1st order and along with additional expressions for the particle velocity u are not adequate in the vicinity of the crest for large values of the ratio $\frac{H}{d}$

$$\frac{u}{\sqrt{gd}} = \frac{H}{d}\operatorname{sech}^2[\sqrt{\frac{3}{4}\frac{H}{d^3}}(x-Ct)] \qquad \text{(II-27)}$$

Munk-McCowan Solitary Wave Theory

This theory[1] is more reliable particularly in the vicinity of the crest of the wave for large values of $\frac{H}{d}$ and provide a better fit to the scanty experimental data. It is however more difficult in computation and the surface pressure is not constant.

$$C \doteq \sqrt{gd(1+\frac{H}{d})} \qquad \text{(II-28)}$$

$$\frac{u}{C} = N[\frac{1-\cos(\frac{My}{d})\cosh(\frac{Mx}{d})}{[\cos(\frac{My}{d})+\cosh(\frac{Mx}{d})]^2}] \qquad \text{(II-29)}$$

where M and N are found from the following:

$$\frac{H}{d} = \frac{N}{M} \tan \frac{1}{2}[M(1+\frac{H}{d})]$$

$$N = \frac{2}{3} \sin^2[M(1+\frac{2}{3}\frac{H}{d})]$$

This theory yields lower values of the dimensionless velocity $\frac{u}{C}$ than the previous one and its generalised third order form.

Cnoidal Theory

This is a nonlinear theory[1] for permanent periodic waves in shallow water where $\frac{d}{L} < \frac{1}{10}$ to $\frac{1}{25}$. Jacobian elliptic functions K(k),E(k),cn u and sn u appear in the expressions, which are involved. The wave period T and height H are independent inputs. Wave length L is given by

$$\frac{L}{d} = \frac{4}{\sqrt{3}} K(k) (2\bar{L}+1-\frac{y_t}{d})^{-1/2} \qquad \text{(II-30)}$$

in which $\bar{L}$ and k are defined by 2 equations as follows:

$$k^2 = \frac{(y_0/d)-(y_t/d)}{2\bar{L}+1-(y_t/d)}$$

$$(2\bar{L}+1-\frac{y_t}{d})E(k) = (2\bar{L}+2-\frac{y_c}{d}-\frac{y_t}{d})K(k) \qquad \text{(Ref.1)}$$

where K(k) = complete elliptic integral of the 1st kind of modulus k

$y_t$ = distance from the ocean bottom to the trough

$y_c$ = distance from the ocean bottom to the crest

E(k) = complete elliptic integral of the 2nd kind of modulus k.

An approximation to L is

$$L = \sqrt{\frac{16d^3}{3H}}\, kK(k) \qquad \text{(II-31)}$$

The wave profile in terms of $y_s$ measured from the bed is given by

$$y_s = y_t + H\, cn^2[2K(k)(\frac{x}{L} - \frac{t}{T}),k]$$

$$= y_t + H\, cn^2[\sqrt{\frac{3}{4}\frac{(2\bar{L}+1-\frac{y_t}{d})}{d^3}}(x-\frac{L}{T}t),k] \qquad \text{(II-32)}$$

The wave velocity $C = \sqrt{gd}[1+\frac{H}{d}\frac{1}{k^2}(\frac{1}{2} - \frac{E(k)}{K(k)}]$ (II-33)

Water particle velocity u:

$$\frac{u}{\sqrt{gd}} = [-\frac{5}{4}+\frac{3y_t}{d}-\frac{y_t^2}{4d^2}+(\frac{3H}{2d} - \frac{y_t H}{2d^2})cn^2(\quad)$$

$$- \frac{H^2}{4d^2}\, cn^4(\quad) - \frac{8HK^2(k)}{L^2}(\frac{d}{3}-\frac{y^2}{2d})\{-k^2 sn^2(\quad)$$

$$cn^2(\quad) + cn^2(\quad)\, dn^2(\quad) - sn^2(\quad)\, dn^2(\quad)\}]$$

where $sn(\quad) \equiv sn[2K(k)(\frac{x}{L} - \frac{t}{T})]$ etc. (II-34)

# APPENDIX III

## RELATIONS FOR THE THIRD ORDER RUNGE--KUTTA METHOD

The system of equations to be solved are rewritten in the form of lst order equations:

$$\dot{u}_i = z_i \qquad i=1,\ldots n \qquad \text{(III-1)}$$

$$\ddot{u}_i = \frac{dz_i}{dt} = \dot{z}_i \qquad i=1,\ldots n \qquad \text{(III-2)}$$

$\dot{z}_i$ is available from the computed values of variables of the preceding step, and through the use of the equations of motion.

For a succeeding time step, the dependent variable u and its first derivative are found as follows:

$$z_i(t+\Delta t) = z_i(t) + \frac{1}{4}\kappa_{i1} + \frac{3}{4}\kappa_{i3} \qquad \text{(III-3)}$$

where $\kappa_{i1} = (\Delta t)\dot{z}_i(z_1, z_2, \ldots z_n, u_1, u_2, \ldots u_n, t)$

$$\kappa_{i2} = (\Delta t)\dot{z}_i(z_1+\tfrac{1}{3}\kappa_{11}, z_2+\tfrac{1}{3}\kappa_{21}, \ldots z_n+\tfrac{1}{3}\kappa_{n1}, u_1+\tfrac{1}{3}q_{11}, u_2+\tfrac{1}{3}q_{21},$$

$$\ldots u_n+\tfrac{1}{3}q_{n1}, t+\tfrac{1}{3}(\Delta t))$$

$$\kappa_{i3} = (\Delta t)\dot{z}_i(z_1+\tfrac{2}{3}\kappa_{12}, z_2+\tfrac{2}{3}\kappa_{22}, \ldots z_n+\tfrac{2}{3}\kappa_{n2}, u_1+\tfrac{2}{3}q_{12}, u_2+\tfrac{2}{3}q_{22},$$

$$\ldots u_n+\tfrac{2}{3}q_{n2}, t+\tfrac{2}{3}(\Delta t)) \qquad \text{(III-4)}$$

$$u_i(t+\Delta t) = u_i(t) + \frac{1}{4}q_{i1} + \frac{3}{4}q_{i3} \qquad \text{(III-5)}$$

where

$$q_{i1} = (\Delta t) z_i$$

$$q_{i2} = (\Delta t)\ (z_i + \tfrac{1}{3}\kappa_{i1})$$

$$q_{i3} = (\Delta t)\ (z_i + \tfrac{2}{3}\kappa_{i2}) \qquad \text{(III-6)}$$

Substituting (III-6) into (III-4) and (III-5), (III-5) is rewritten

$$u_i(t+\Delta t) = u_i(t) + (\Delta t) z_i(t) + \tfrac{1}{2}\ (\Delta t)\kappa_{i2} \qquad \text{(III-7)}$$

and

$$\begin{aligned}
\kappa_{i1} &= (\Delta t)\dot{z}_i[z_1(t), z_2(t), z_3(t) \ldots z_n(t), u_1(t), u_2(t), \\
&\quad \ldots u_n(t), t] \\
\kappa_{i2} &= (\Delta t)\dot{z}_i[z_1+\tfrac{1}{3}\kappa_{11}, z_2+\tfrac{1}{3}\kappa_{21}, \ldots z_n+\tfrac{1}{3}\kappa_{n1}, u_1+\tfrac{1}{3}(\Delta t) z_1, \\
&\quad u_2+\tfrac{1}{3}(\Delta t) z_2, \ldots u_n+\tfrac{1}{3}(\Delta t) z_n, t+\tfrac{1}{3}(\Delta t)] \\
\kappa_{i3} &= (\Delta t)\dot{z}_i[z_1+\tfrac{2}{3}\kappa_{12}, z_2+\tfrac{2}{3}\kappa_{22}, \ldots z_n+\tfrac{2}{3}\kappa_{n2}, \\
&\quad u_1+\tfrac{2}{3}(\Delta t) z_1+\tfrac{2}{9}(\Delta t)\kappa_{11}, u_2+\tfrac{2}{3}(\Delta t) z_2+\tfrac{2}{9}(\Delta t)\kappa_{21}, \\
&\quad \ldots u_n+\tfrac{2}{3}(\Delta t) z_n+\tfrac{2}{9}(\Delta t)\kappa_{n1}, t+\tfrac{2}{3}(\Delta t)] \qquad \text{(III-8)}
\end{aligned}$$

(III-3), (III-7), and (III-8) are explicit formulae.

The above set of equations are part of one form of the third order Runge-Kutta relations for a particular choice of parameters.